ACSNANO

www.acsnano.org

ARTICLE

Biomimetic Mechanically Strong One-Dimensional Hydroxyapatite/Poly(D,L-lactide) Composite Inducing Formation of Anisotropic Collagen Matrix

Yonggang Zhang, Jiaping Li, Vivian Hilda Maria Mouser, Nadia Roumans, Lorenzo Moroni, and Pamela Habibovic*

Cite This: *ACS Nano* 2021, 15, 17480–17498

Read Online

ACCESS | Metrics & More | Article Recommendations | Supporting Information

ABSTRACT: **Natural bone is a complex composite, consisting predominantly of collagen and hydroxyapatite (HA), which form a highly organized, hierarchical structure from the nano- to the macroscale. Because of its biphasic, anisotropic, ultrafine structural design, bone tissue possesses excellent mechanical properties. Herein, inspired by the composition and microstructure of natural bone, a biphasic composite consisting of highly aligned strontium/copper-doped one-dimensional hydroxyapatite (Sr/Cu-doped 1D HA) and poly(D,L-lactide) (PDLA) was developed. The presence and alignment of Sr/Cu-doped 1D HA crystals resulted in mechanical reinforcement of the polymer matrix, including compressive and tensile strength and modulus, fracture toughness, swelling resistance, and long-term structural stability. The compressive strength, tensile strength, and Young's modulus of the biomimetic composite were comparable to that of cortical bone. Biologically, the biomimetic composite showed a sustained release of the incorporated Sr and Cu ions, facilitated mineral deposition from simulated body fluid, and supported attachment, proliferation, and alkaline phosphatase activity of human mesenchymal stromal cells (hMSCs). Moreover, the highly aligned Sr/Cu-doped 1D HA crystals in the 3D porous scaffolds induced the alignment of hMSCs and secretion of an anisotropic collagen fiber matrix in 3D. The biomimetic Sr/Cu-doped 1D HA/PDLA composite presented here contributes to the current efforts aiming at the design and development of load-bearing bioactive synthetic bone graft substitutes. Moreover, the biomimetic composite may serve as a 3D platform for studying cell−extracellular matrix interactions in bone tissue.**

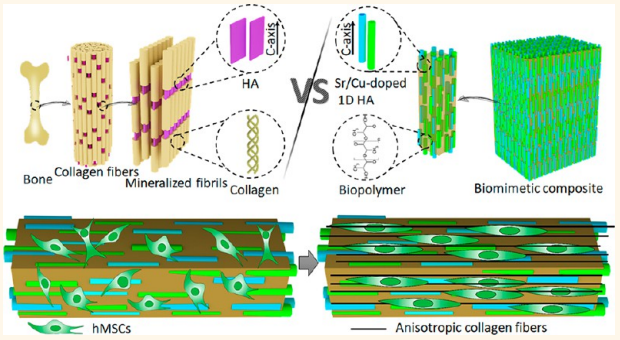

KEYWORDS: *bone, biomimetic, composite, hydroxyapatite, PDLA, anisotropy*

INTRODUCTION

In the fields of orthopedics and craniomaxillofacial surgery, large bone defects and bone loss resulting from severe trauma, tumor resection, infection, and other diseases pose a great clinical challenge worldwide, causing pain to the patients, decreasing quality of life, and even reducing life expectancy.[1−3] It is estimated that over four million bone grafts are used annually worldwide.[4] To address this challenge, it is important to develop biomaterials that can be used as an effective replacement of a patient's own bone transplants, which have limited availability.

From a materials perspective, natural bone is a complex composite, consisting predominantly of collagen and calcium phosphate (CaP) in the form of nanocrystalline hydroxyapatite (HA).[5,6] Collagen nanofibrils are the main constituent of the organic matrix, endowing natural bone with excellent tensile strength and toughness, while HA nanocrystals, the inorganic phase, provide high stiffness and high compressive strength and act as a natural reservoir of calcium, phosphate, and other inorganic ions. As a biomimetic approach to develop synthetic bone graft substitutes, in the last 40 years, extensive research

Received: May 8, 2021
Accepted: October 13, 2021
Published: October 18, 2021

https://doi.org/10.1021/acsnano.1c03905
ACS Nano 2021, 15, 17480−17498

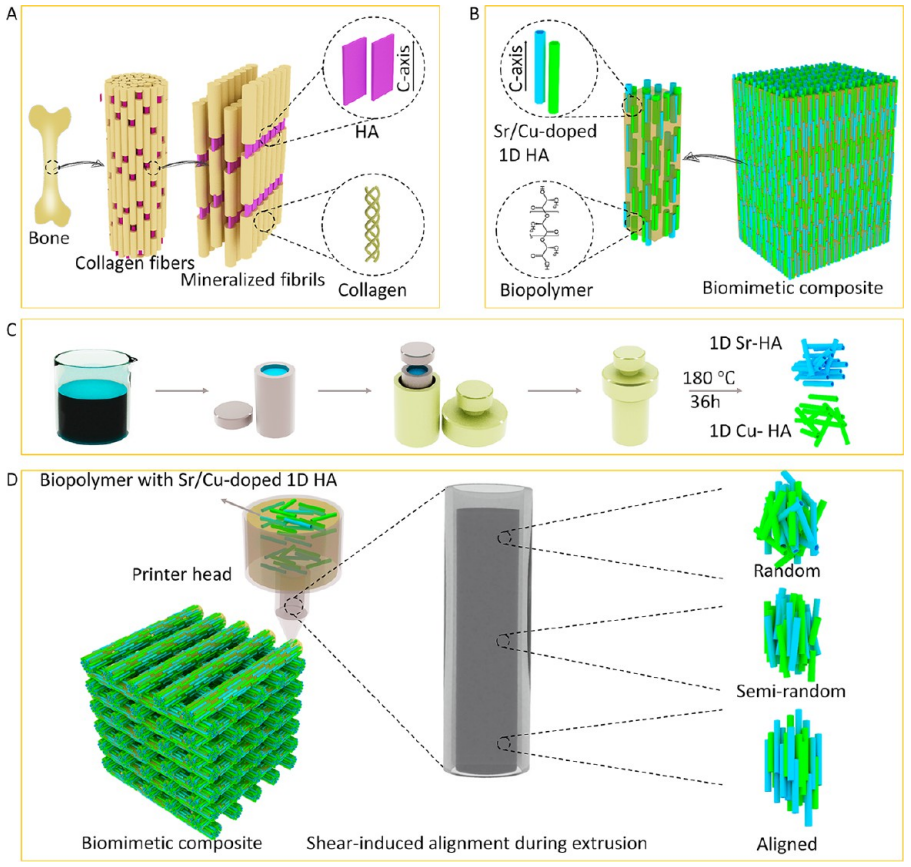

Figure 1. Schematic illustration of the (A) microstructure of natural bone, (B) design of the biomimetic composite, (C) preparation process of the 1D Sr-HA and 1D Cu-HA, and (D) fabrication process of the biomimetic composite.

efforts have been expended to synthesize and fabricate composites consisting of various polymers and CaP phases.[7] For example, successful development of composites combining CaPs with collagen,[8,9] chitosan,[10,11] alginate,[12,13] poly(caprolactone) (PCL),[14,15] poly(lactic acid) (PLA),[16−18] poly(ether ether ketone) (PEEK), and poly(urethane) (PU)[19−21] has been demonstrated. Importantly, the mechanical properties of these composites are rarely comparable to those of natural bone. Moreover, the mechanical properties, such as tensile strength and bending strength of some polymers, decreased rather than increased by blending them with CaP into a composite.[22−24]

An important reason for this is the fact that, while much attention was paid to the actual choice of the polymer and ceramic phase, *e.g.*, to tailor their degradation and bioactivity, less attention was paid to the structural characteristics of the individual components and their spatial organization in the composite material. A majority of the composites developed for applications in bone repair and regeneration are made by either physical mixing of the polymer and ceramic (nano)particles or by adding the ceramic (nano)particles to a dissolved polymer, followed by processes such as freeze-drying or extrusion. As a result, in general, a random, aggregated, unstructured distribution of the ceramic particles in the composite was observed, which is very different from the structure of natural bone.[16,18,21,25,26]

In fact, the superior mechanical properties of natural bone are attributed not only to its chemical composition, but largely to its hierarchical structural design. On the micro- and nanoscale, bone comprises uniaxial, highly aligned collagen nanofibrils with HA nanocrystals embedded in a spatially controlled manner to serve as reinforcement. These HA nanocrystals are oriented such that the crystallographic *c*-axes lie parallel to the long axes of the collagen fibrils and their (1 0 0) planes are all approximately parallel to each other.[27−29] Because of this highly aligned, anisotropic, biphasic, ultrafine structural design, bone tissue possesses excellent tensile strength and toughness, as well as high stiffness and compressive strength.[28,30] Therefore, it is important to investigate how microstructure influences the mechanical properties and bioactivity of the polymer/CaP composites and use this knowledge to develop bone graft substitutes that more closely resemble natural bone tissue. A few attempts have been made in this direction including the development of polymer fiber-reinforced CaP cements, intrafibrillar collagen mineralization, and composites produced by *in situ* CaP precipitation. Polymer fibers were successfully introduced into CaP cements; however, their spatial distribution was poorly controlled and their reinforcement effect, in terms of improved elasticity modulus and flexural strength, was limited.[31−33] Biomimetic methods of intrafibrillar collagen mineralization resulted in hierarchical collagen/HA fibers with bone-like microstructure; however, this biomimetic structure was restricted to the single-fiber level rather than the scaffold as a whole, due to the fabrication methods used.[34,35] The *in situ* mineral precipitation method delivered a polymer/CaP composite with homogeneously distributed HA nanoparticles. Nevertheless, the spatial arrangement of these HA nanoparticles was random and different from that of natural bone.[36,37]

https://doi.org/10.1021/acsnano.1c03905
ACS Nano 2021, 15, 17480−17498

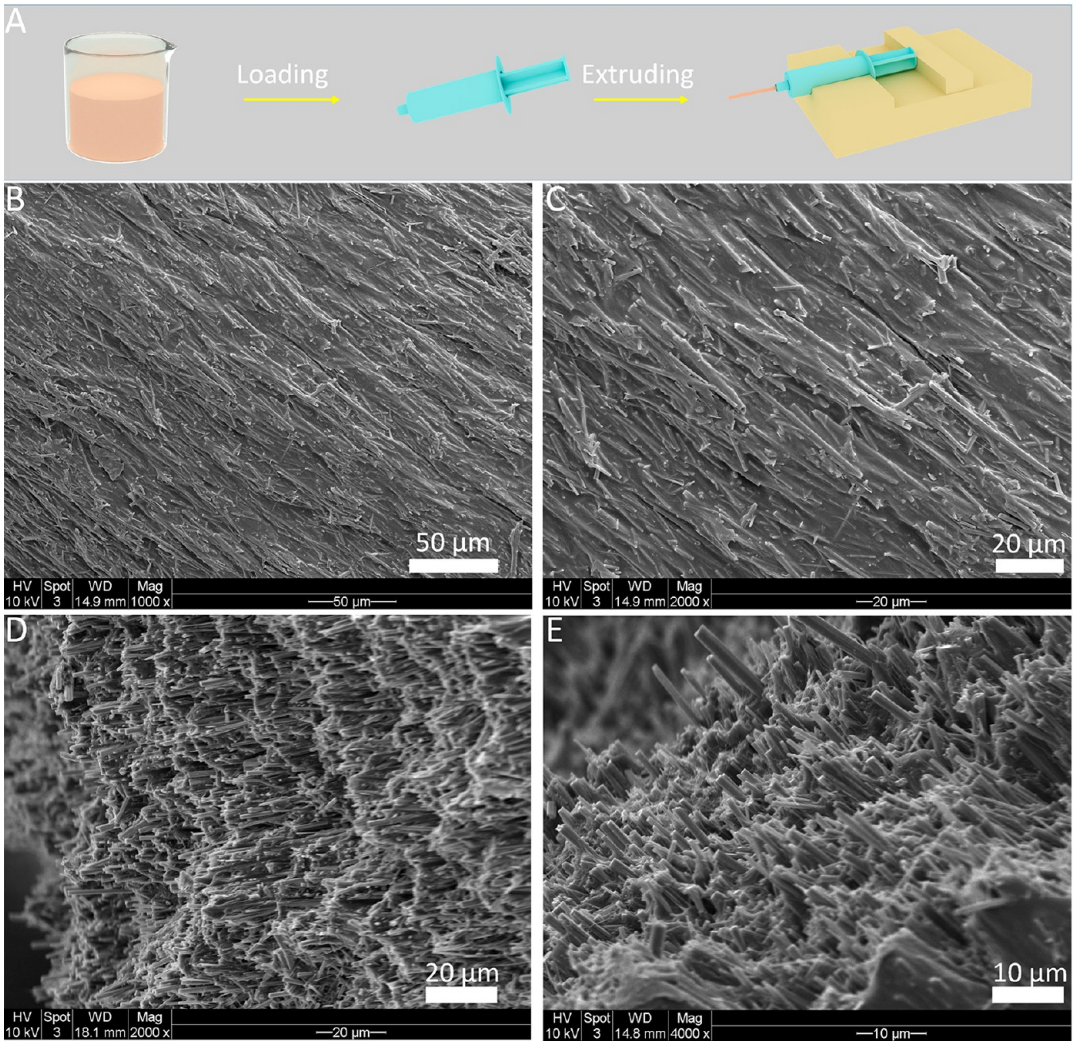

Figure 2. (A) Schematic illustration of the fabrication process of Sr/Cu-doped 1D HA/PCL filaments by using a syringe. SEM micrographs of the surface (B, C) and cross-section (D, E) of the Sr/Cu-doped 1D HA/PCL filament obtained by extruding a suspension with the solid content of 33.3 wt % using an 18G needle with a length of 10 mm at the extrusion rate of 100 μL/min.

Herein, inspired by natural bone, we have developed a biomimetic composite consisting of strontium (Sr)/copper (Cu)-doped 1D HA and poly(DL-lactide) (PDLA), which not only exhibits mechanical properties comparable to those of natural bone but also serves as a 3D platform for the study of bone cell−matrix interactions. In the Sr/Cu-doped 1D HA/PDLA composite, PDLA forms the organic matrix, while uniformly dispersed, highly aligned Sr/Cu-doped 1D HA crystals embedded in the PDLA matrix serve as an inorganic reinforcement phase, just like the HA nanocrystals in natural bone. Mechanically, the existence of aligned Sr/Cu-doped 1D HA crystals resulted in all-sided mechanical reinforcement of the polymer matrix, including compression, tension, modulus, fracture toughness, swelling resistance, and long-term mechanical stability. Biologically, the biomimetic composite showed a sustained release of the incorporated Sr and Cu ions and supported proliferation and alkaline phosphatase activity of human mesenchymal stromal cells (hMSCs). Interestingly, the oriented Sr/Cu-doped 1D HA induced the alignment of hMSCs throughout the scaffold and production of an anisotropic type I collagen fiber matrix. The method and design principles applied here may provide inspiration for other researchers developing advanced composites for bone regeneration.

RESULTS AND DISCUSSION

Biomimetic Design of Sr/Cu-Doped 1D HA/Biopolymer Composite. Natural bone comprises uniaxial, highly aligned collagen nanofibrils mineralized with HA nanocrystals that are aligned along their crystallographic *c*-axes and lie parallel to the long axes of the collagen fibrils (Figure 1A). Inspired by this, herein, we aimed at developing a synthetic composite to mimic natural bone from both a compositional and structural perspective. As is shown in Figure 1B, the biomimetic composite design included a biphasic organic/inorganic composition consisting of Sr/Cu-doped 1D HA and linear biopolymer (PCL or PDLA). The ceramic crystals were designed to be uniformly distributed within the polymer matrix and highly aligned along their crystallographic *c*-axes, similar to HA nanocrystals in natural bone. The fabrication process of the biomimetic composite is shown in Figure 1, C and D. First, 1D Sr-HA and 1D Cu-HA were prepared through a hydrothermal method (Figure 1C). Biological HA, as found in bone, is not stoichiometric and contains several additional elements, often in trace amounts, such as Sr, potassium,

https://doi.org/10.1021/acsnano.1c03905
ACS Nano 2021, 15, 17480−17498

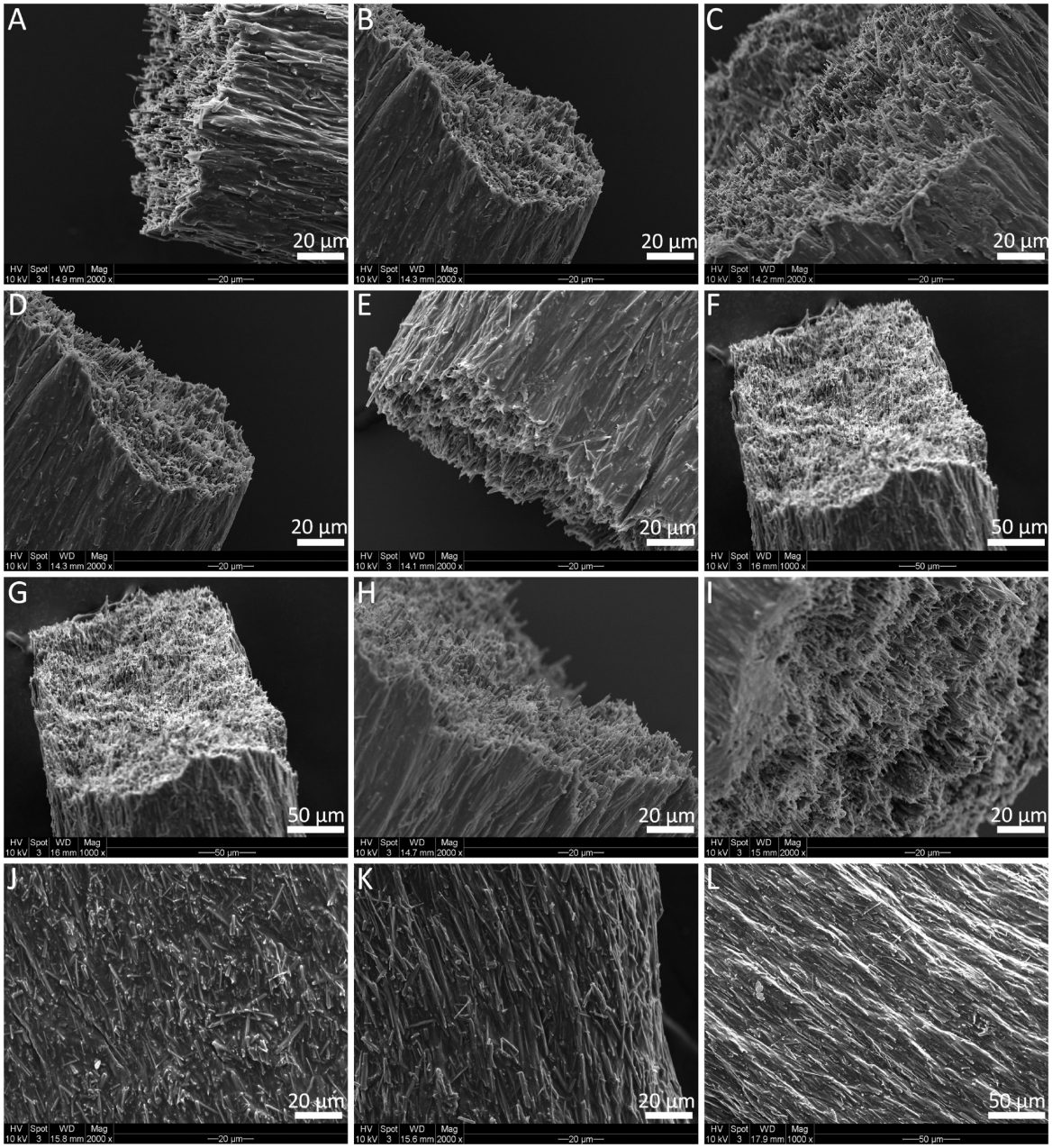

Figure 3. (A to C) SEM micrographs of Sr/Cu-doped 1D HA/PCL filaments obtained by extruding a suspension with the solid content of 33.3 wt % at the extrusion rate of 100 μL/min using needles with a length of 10 mm but different diameter (25G, 21G, 18G, respectively). (D to F) SEM micrographs of Sr/Cu-doped 1D HA/PCL filaments obtained by extruding a suspension with the solid content of 33.3 wt % at the extrusion rate of 100 μL/min using 21G needles with different lengths (2, 6, 10 mm, respectively). (G to I) SEM micrographs of Sr/Cu-doped 1D HA/PCL filaments obtained by extruding a suspension with the solid content of 33.3 wt % by using the same needle (21G, 2 mm) but three different extrusion rates (100, 200, 400 μL/min, respectively). (J to L) SEM micrographs of Sr/Cu-doped 1D HA/PCL filaments obtained by using the same needle (21G, 2 mm) and the same extrusion rate (100 μL/min) but three different concentrations of the solid content of the suspension (24.4, 33.3, 42.3 wt %, respectively).

fluoride, zinc, magnesium, carbonate, and silicate, which play an important role in bone metabolism.[38] Moreover, many ions including Sr, Cu, zinc, cobalt, and sodium were reported to affect processes related to bone regeneration.[39] For example, Sr ions have been shown to enhance the osteogenic differentiation of hMSCs and to inhibit proliferation of osteoclasts.[40,41] Cu ions have been suggested to enhance the expression of angiogenic and osteogenic markers in hMSCs, as well as to provide antibacterial effects.[42,43] Therefore, herein, we incorporated Sr and Cu ions into the 1D HA as a biomimetic way to enhance the bioactivity of the composite. The 1D Sr-HA and 1D Cu-HA were both phase-pure HA crystals with a length of around 50 micrometers and a diameter of about one micrometer (Figure S1, Supporting Information). The amount of Sr and Cu in the 1D Sr-HA and 1D Cu-HA, as determined using inductively coupled plasma-mass spectrometry (ICP-MS), was 10.2% (Sr/(Ca + Sr), mole ratio) and 4.6% (Cu/(Ca + Cu), mole ratio), respectively. In the second step, Sr/Cu-doped 1D HA consisting of 50 wt % 1D Sr-HA and 50 wt % 1D Cu-HA was mixed with biopolymer (PCL or

https://doi.org/10.1021/acsnano.1c03905
ACS Nano 2021, 15, 17480−17498

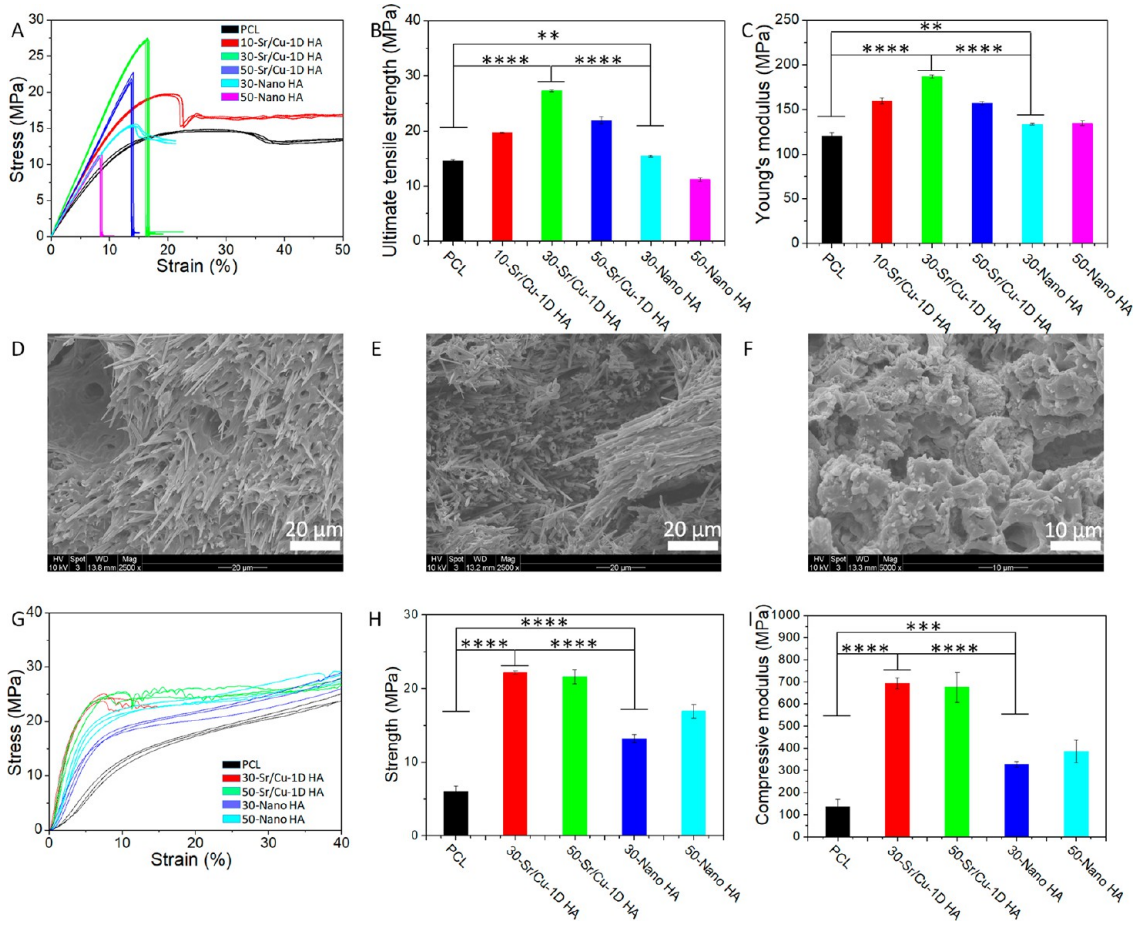

Figure 4. (A–C) Tensile stress–strain curves, UTS, and Young's modulus of pure PCL, biomimetic Sr/Cu-doped 1D HA/PCL composites with 10, 30, and 50 wt % Sr/Cu-doped 1D HA, and Nano HA/PCL composites with 30 and 50 wt % Nano HA, respectively. (D–F) SEM micrographs of the fracture surface of biomimetic Sr/Cu-doped 1D HA/PCL composites with 30 and 50 wt % Sr/Cu-doped 1D HA and the Nano HA/PCL composite with 50 wt % Nano HA after the tensile test, respectively. (G–I) Compressive stress–strain curves, compressive strength (at 5% strain), and compressive modulus of pure PCL, biomimetic Sr/Cu-doped 1D HA/PCL composites with 30 and 50 wt % Sr/Cu-doped 1D HA, and Nano HA/PCL composites with 30 and 50 wt % Nano HA in the longitudinal direction, respectively. (*) for $p < 0.05$, (**) for $p < 0.01$, (***) for $p < 0.001$, and (****) for $p < 0.0001$.

PDLA) to form a uniform mixture, then extruded through a nozzle by using a 3D plotting system. During the extrusion process, the orientation of Sr/Cu-doped 1D HA changed gradually from random to highly aligned due to the shear stress within the suspension flow (Figure 1D). Similarly, shear stress-induced alignment of anisotropic materials such as cellulose nanocrystals and carbon fibers was reported elsewhere.[44,45] Finally, by controlling the movement of the printer head, the biomimetic composite with desired dimensions and shape was obtained.

Anisotropic Structure of the Biomimetic Composite. First, we chose PCL as the polymer matrix to investigate whether it is possible to obtain composites with aligned Sr/Cu-doped 1D HA. As is shown in Figure 2A, a suspension of Sr/Cu-doped 1D HA (50 wt %) and PCL (50 wt %) with a concentration of the solid content of 33.33 wt % in chloroform was prepared and loaded in a 5 mL syringe. The suspension was then extruded through a needle (18G, 10 mm) at the speed of 100 μL/min under the control of a syringe pump. The orientation of Sr/Cu-doped 1D HA within the PCL matrix was characterized using a scanning electron microscope (SEM). Figure 2, B to E, show that the Sr/Cu-doped 1D HA crystals were uniformly embedded in the PCL matrix and were highly aligned along the long axes of the extruded filament throughout the entire structure. Furthermore, the effects of the diameter and length of the needle, the extrusion rate, and the concentration of the solid content on the alignment of Sr/Cu-doped 1D HA were investigated. First, three needles with different diameters (25G, 21G, 18G) were tested while keeping the other parameters constant. Figure 3, A to C, show that aligned Sr/Cu-doped 1D HA was successfully obtained in the PCL matrix with all needles, indicating that the diameter of the needle did not have an obvious effect on the microstructure of the composite filament. The results showed no obvious effects of either the length of the needle (Figure 3, D to F) or the extrusion rate (Figure 3, G to I) on the ceramic alignment. The concentration of the solid content seemed to be the dominant factor that influenced the alignment of Sr/Cu-doped 1D HA. As shown in Figure 3, J to L, the Sr/Cu-doped 1D HA crystals were less aligned when the concentration of the solid content was 24.4 wt % (Figure 3J) than when the concentration of the solid content was 33.3 wt % (Figure 3K) or 42.3 wt % (Figure 3L). This phenomenon could be explained by the change of viscosity of the suspension when the concentration of the solid content changed. The viscosity of the suspension was difficult to quantify due to the very fast

https://doi.org/10.1021/acsnano.1c03905
ACS Nano 2021, 15, 17480–17498

volatilization of chloroform. However, the suspension with the solid content of 42.3 wt % was observed to have the highest viscosity (hardest to stir by hand), and as a result, a higher shear stress was exerted on the suspension during extrusion, in turn resulting in a more pronounced alignment of Sr/Cu-doped 1D HA inside the polymer matrix.

Mechanical Properties of the Biomimetic Sr/Cu-Doped 1D HA/PCL Compact Samples. To investigate the effect of incorporation of aligned Sr/Cu-doped 1D HA into the polymer, the tensile and compressive properties of compact biomimetic composite samples were investigated, using compact samples of Nano HA/PCL (composite prepared using conventional nanosized HA particles) and pure PCL as controls.

First, the tensile test was performed by applying force on the sample in the direction in which Sr/Cu-doped 1D HA crystals were aligned. The tensile stress−strain curves and ultimate tensile strength (UTS) are shown in Figure 4, A and B. The UTS of the composite increased with the increase of the amount of Sr/Cu-doped 1D HA and reached the highest value when the amount of Sr/Cu-doped 1D HA was 30 wt %. The UTS of the composite with 30 wt % ceramic was 1.87 times higher than that of pure PCL. The UTS of the Nano HA/PCL composite with the same amount of HA was significantly lower than that of the biomimetic Sr/Cu-doped 1D HA/PCL composites (Figure 4B; Table S1, Supporting Information). The UTS of the Nano HA/PCL composite with 30 wt % HA was comparable to that of pure PCL, but when the ceramic content was increased to 50 wt %, the UTS of the composite was about 23% lower than that of the polymer without ceramic. In contrast, the biomimetic Sr/Cu-doped 1D HA/PCL composite with 50 wt % ceramic showed an increase of UTS of about 50% compared to pure PCL (Figure 4B; Table S1, Supporting Information).

The Young's modulus of the pure PCL, the biomimetic Sr/Cu-doped 1D HA/PCL composites, and the Nano HA/PCL composites is shown in Figure 4C and Table S1. Again, the biomimetic Sr/Cu-doped 1D HA/PCL composites with 30 wt % Sr/Cu-doped 1D HA showed the highest Young's modulus, which was about 1.5 times higher than that of pure PCL.

The morphology of the fracture area of the samples after the tensile test was observed by SEM (Figure 4, D to F). Sr/Cu-doped 1D HA crystals were observed on the fracture surface of the biomimetic Sr/Cu-doped 1D HA/PCL composite with 30 wt % ceramic content. On one side of the fractured sample, Sr/Cu-doped 1D HA was still embedded in the PCL matrix, while on the other end, the crystals were exposed, suggesting that the crystals were pulled out from the other part of the sample during the tensile test (Figure 4D). It is suggested that the interfacial debonding between Sr/Cu-doped 1D HA and PCL matrix and the pull out of Sr/Cu-doped 1D HA from the PCL matrix resulted in absorption of crack-propagating energy, which was increased because of the alignment of the ceramic phase in the composite. This is plausibly the reason for the biomimetic Sr/Cu-doped 1D HA/PCL composite with 30 wt % Sr/Cu-doped 1D HA showing higher UTS and Young's modulus than the other tested materials.

In the case of the biomimetic composite with 50 wt % Sr/Cu-doped 1D HA, many small bundles of Sr/Cu-doped 1D HA/PCL were observed in the fracture area (Figure 4E). Because of the relatively high ceramic content, the polymer was not the dominant phase of the composite anymore. As a result, the strength of the PCL matrix decreased and during the tensile test the composite was prone to break at the PCL matrix framework, thus leaving bundles of Sr/Cu-doped 1D HA/PCL on the fracture surface (Figure S2, Supporting Information). As a result, the UTS and Young's modulus of the biomimetic Sr/Cu-doped 1D HA/PCL composite with 50 wt % Sr/Cu-doped 1D HA were somewhat lower than those of the Sr/Cu-doped 1D HA/PCL composite with 30 wt % Sr/Cu-doped 1D HA. Due to the low aspect ratio and random distribution of the Nano HA, the effect of interfacial debonding between Nano HA and the PCL matrix and pull-out of the Nano HA from the PCL matrix were negligible during the tensile test. Therefore, only irregular fragments of the composite were found on the fracture surface of the Nano HA/PCL composite with 50 wt % Nano HA (Figure 4F). As a consequence, the tensile properties of the nano HA/PCL composites were inferior to those of biomimetic Sr/Cu-doped 1D HA/PCL composites.

The compressive test on the compact composite and pure PCL samples was performed by using a uniaxial compression testing equipment. The compressive strength of the compact Sr/Cu-doped 1D HA/PCL composites was analyzed both in the longitudinal direction, in which the aligned Sr/Cu-doped 1D HA crystals inside the composite were parallel to the *z*-axis, and in transversal direction, where the Sr/Cu-doped 1D HA crystals in the composite were perpendicular to the *z*-axis (Figure S3, A and B, Supporting Information). The compressive stress−strain curves of the biomimetic Sr/Cu-doped 1D HA/PCL compact composite samples loaded in the longitudinal direction are shown in Figure 4G. Pure PCL and the Nano HA/PCL composite with the same amount of HA were used as controls. Similar to the results of the tensile test, the biomimetic Sr/Cu-doped 1D HA/PCL composites exhibited the highest compressive strength (Figure 4H) and highest compressive modulus (Figure 4I) among the groups. The compressive modulus of the Sr/Cu-doped 1D HA/PCL composite with 30 wt % Sr/Cu-doped 1D HA was about 5 times higher than that of pure PCL (Table S2, Supporting Information). The anisotropic structure of the biomimetic Sr/Cu-doped 1D HA/PCL composites resulted in anisotropic mechanical properties (Figure S3, C and D, Supporting Information). The compressive strength and compressive modulus of the Sr/Cu-doped 1D HA/PCL composite with 30 wt % Sr/Cu-doped 1D HA in the transversal direction were significantly lower than those in the longitudinal direction. When the loading was applied in the longitudinal direction, the ceramic crystals acted as "pillars" that bear the load efficiently, hence resulting in higher compressive strength and higher compressive modulus in this direction. This reinforcement effect disappeared when the loading was applied in the transversal direction (on the sides of the "pillars"), leading to a significant decrease of the compressive strength and compressive modulus.

Mechanical Properties of the Biomimetic Sr/Cu-Doped 1D HA/PDLA Compact Samples. The mechanical properties of the biomimetic Sr/Cu-doped 1D HA/PCL composite were significantly improved by introducing highly aligned Sr/Cu-doped 1D HA into the polymer matrix. Nevertheless, these properties were still inferior to those of natural bone. Therefore, in this part, we changed the polymer matrix of the biomimetic composite from PCL to PDLA and developed a biomimetic Sr/Cu-doped 1D HA/PDLA composite, since the elasticity modulus of PDLA is higher than that of PCL.[46] Compact samples of Sr/Cu-doped 1D

https://doi.org/10.1021/acsnano.1c03905
ACS Nano 2021, 15, 17480−17498

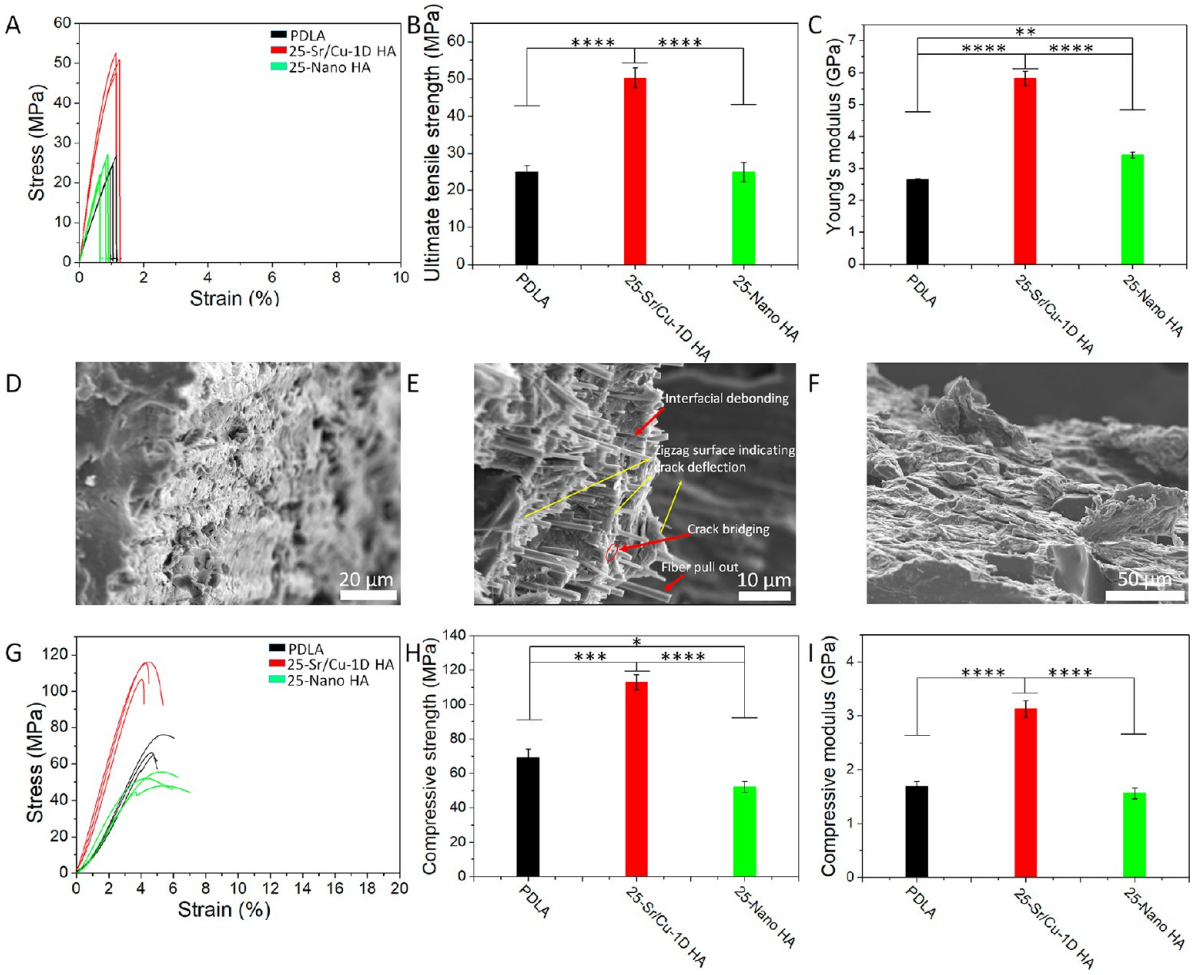

Figure 5. (A–C) Tensile stress–strain curves, UTS, and Young's modulus of pure PDLA, the biomimetic Sr/Cu-doped 1D HA/PDLA composite with 25 wt % Sr/Cu-doped 1D HA, and the Nano HA/PDLA composite with 25 wt % Nano HA, respectively. (D–F) SEM micrographs of the fracture surface after the tensile test of pure PDLA, the biomimetic Sr/Cu-doped 1D HA/PDLA composite with 25 wt % Sr/Cu-doped 1D HA, and the Nano HA/PDLA composite with 25 wt % Nano HA, respectively. (G–I) Compressive stress–strain curves, compressive strength, and compressive modulus of pure PDLA, the biomimetic Sr/Cu-doped 1D HA/PDLA composite with 25 wt % Sr/Cu-doped 1D HA, and the Nano HA/PDLA composite with 25 wt % Nano HA, respectively. (*) for $p < 0.05$, (**) for $p < 0.01$, (***) for $p < 0.001$, and (****) for $p < 0.0001$.

HA/PDLA composite were prepared by extruding the mixture of Sr/Cu-doped 1D HA/PDLA through a heated nozzle, similar to the preparation of the composite with PCL. According to the results of the mechanical tests of the Sr/Cu-doped 1D HA/PCL composites, the optimal amount of Sr/Cu-doped 1D HA in the polymer matrix was determined to be 30 wt %. However, we decreased the amount of Sr/Cu-doped 1D HA in the PDLA matrix from 30 wt % to 25 wt % since it was difficult to extrude the Sr/Cu-doped 1D HA/PDLA mixture through a nozzle with a higher amount of the ceramic. Similar to the microstructure of the Sr/Cu-doped 1D HA/PCL composite, the Sr/Cu-doped 1D HA crystals were highly aligned in the PDLA matrix (Figure S4, Supporting Information).

The tensile stress–strain curves of compact Sr/Cu-doped 1D HA/PDLA samples, upon applying tensile force in the direction of Sr/Cu-doped 1D HA alignment, are shown in Figure 5A. Pure PDLA and the Nano HA/PDLA composite with the same amount of HA were used as controls. The UTS of the biomimetic Sr/Cu-doped 1D HA/PDLA composite was significantly higher than that of pure PDLA and Nano HA/PDLA (Figure 5B). The Young's modulus of the biomimetic Sr/Cu-doped 1D HA/PDLA composite was as high as 6.1 GPa and, again, significantly higher than that of pure PDLA and Nano HA/PDLA samples (Figure 5C; Table S3, Supporting Information). The SEM images of the fracture surface of the samples after the tensile test (Figure 5, D to F) showed that the surface of PDLA (Figure 5D) and the Nano HA/PDLA composite (Figure 5F) was relatively smooth. In contrast, the surface of the biomimetic composite was irregular with Sr/Cu-doped 1D HA crystals exposed on it. The pull out and crack bridging effect of Sr/Cu-doped 1D HA crystals, the interfacial debonding between Sr/Cu-doped 1D HA crystals and the PDLA matrix, and the crack deflection effect induced by Sr/Cu-doped 1D HA crystals contributed to the increase in tensile properties of the composite (Figure 5E).

The compressive stress–strain curves of the biomimetic Sr/Cu-doped 1D HA/PDLA composite, upon loading in the longitudinal direction, are shown in Figure 5G. The incorporation of the aligned Sr/Cu-doped 1D HA resulted in an increase of the compressive strength of PDLA from 69 MPa to 113 MPa (Figure 5H) and an improvement of 85% of the compressive modulus (Figure 5I; Table S4, Supporting

https://doi.org/10.1021/acsnano.1c03905
ACS Nano 2021, 15, 17480–17498

Information). The effect of incorporation of Nano HA on the mechanical reinforcement of the polymer was limited.

The fracture toughness (K_Q) of compact Sr/Cu-doped 1D HA/PDLA samples upon applying bending force in the direction perpendicular to the Sr/Cu-doped 1D HA alignment was characterized *via* single-edge-notch bending (SENB) testing. Pure PDLA and the Nano HA/PDLA composite with the same amount of HA were used as controls. As shown in Figure S5 (Supporting Information), the fracture toughness of Sr/Cu-doped 1D HA/PDLA was 2.37 MPa·m$^{1/2}$, which was significantly higher than that of pure PDLA (1.03 MPa·m$^{1/2}$) and was higher, although not statistically significant, than that of the Nano HA/PDLA composite (1.35 MPa·m$^{1/2}$).

Taken together, by introducing highly aligned Sr/Cu-doped 1D HA into the polymer matrix, the mechanical properties including tensile strength, compressive strength, compressive modulus, and fracture toughness of the material were significantly improved.

The biomimetic microstructure endowed the Sr/Cu-doped 1D HA/PDLA with an all-round improvement of mechanical properties including compressive strength, tensile strength, Young's modulus, and fracture toughness. The reinforcement efficiency (102.2%) of tensile strength of the biomimetic Sr/Cu-doped 1D HA/PDLA composite was higher than that of other HA/PLA composites reported in the literature (Figure 6A; Table S5, Supporting Information). It is important to note that the biomimetic Sr/Cu-doped 1D HA/PDLA composite showed high compressive strength (116 MPa) and high Young's modulus (6.1 GPa) even though it was made from PDLA with a relatively low molecular weight (Figure 6B; Table S6, Supporting Information). A comparison with physical properties of cortical bone (Table 1) showed similarities in compressive strength, tensile strength, Young's modulus, and density.

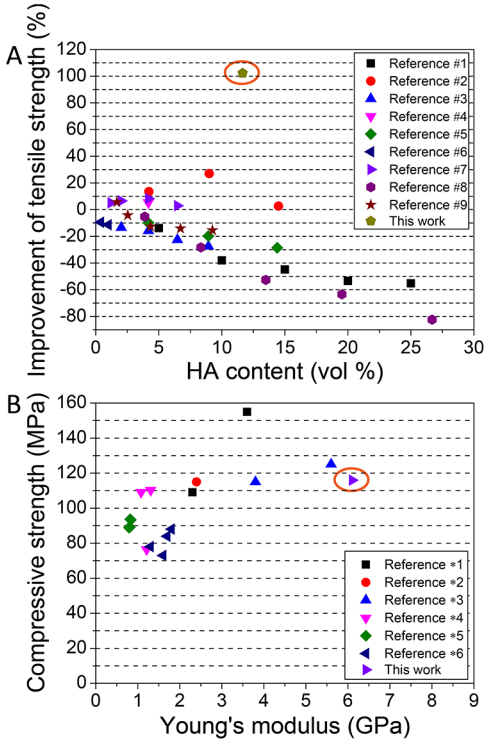

Figure 6. Comparison of reinforcement efficiency of (A) tensile and (B) compressive strength of HA/PLA composites between this and previously published work (more information and references can be found in Table S5 and Table S6).

Table 1. Physical Properties of the Biomimetic Sr/Cu-Doped 1D HA/PDLA Composite and Cortical Bone

material	compressive strength (MPa)	tensile strength (MPa)	Young's modulus (GPa)	density (g/cm^3)	ref
cortical bone	100−230	50−151	7−30	1.6−2.1	47, 48
biomimetic Sr/Cu-doped 1D HA/PDLA composite	116	52.6	6.1	1.32	this work

Mechanical Properties of Sr/Cu-Doped 1D HA/PDLA Porous Scaffolds. In the context of bone graft substitutes, biodegradable materials are required that support the regeneration process (in an ideal situation both mechanically and biologically) and during the process degrade without leaving remnants in the body that may cause long-term adverse effects. Nevertheless, biomaterial degradation, especially when biodegradable polymers are used, may deteriorate the mechanical properties of the bone graft substitute, thereby impairing the process of regeneration.[49] Therefore, one of the ultimate challenges in bone regeneration is to achieve a balance between tissue formation and biomaterial degradation.[50] In addition to degradation properties, swelling behavior is another important factor that influences the physical properties of the polymer-based bone graft substitutes before and after implantation. Uncontrolled swelling can be detrimental to the mechanical properties of the implant.[51] Therefore, we set out to investigate the swelling behavior and its effect on the mechanical properties of Sr/Cu-doped 1D HA/PDLA porous scaffolds.

Sr/Cu-doped 1D HA/PDLA porous scaffolds with a porosity of 50% were prepared by layer-by-layer printing in the 0−90 deg direction. The schematic illustration of the structure of the porous scaffolds is shown in Figure S6 (Supporting Information). Due to the anisotropic distribution of the Sr/Cu-doped 1D HA, the mechanical properties of the Sr/Cu-doped 1D HA/PDLA porous scaffolds were also anisotropic. The compressive stress−strain curves of the Sr/Cu-doped 1D HA/PDLA porous scaffolds in the longitudinal and transversal direction (Figure S7A, Supporting Information) are shown in Figure S7B (Supporting Information). The compressive strength of the Sr/Cu-doped 1D HA/PDLA porous scaffolds in the transversal direction was higher than that in the longitudinal direction. The Sr/Cu-doped 1D HA/PDLA porous scaffolds could bear the load consistently and showed better structural stability when loaded in the transversal direction. The reason for this observation may be the fact that the layers were more prone to detach during the compression test in the longitudinal direction than in the transversal direction, as is illustrated in Figure S8, Supporting Information, thus resulting in an inferior structural stability in the longitudinal direction. For the rest of this section, the results reported are based on compression tests with loading applied in the transversal direction, unless otherwise stated. Figure 7A shows that the Sr/Cu-doped 1D HA/PDLA porous scaffolds exhibited a higher compressive strength and better structural stability than scaffolds made of pure PDLA and Nano HA/PDLA that served as controls. In contrast to porous

https://doi.org/10.1021/acsnano.1c03905
ACS Nano 2021, 15, 17480−17498

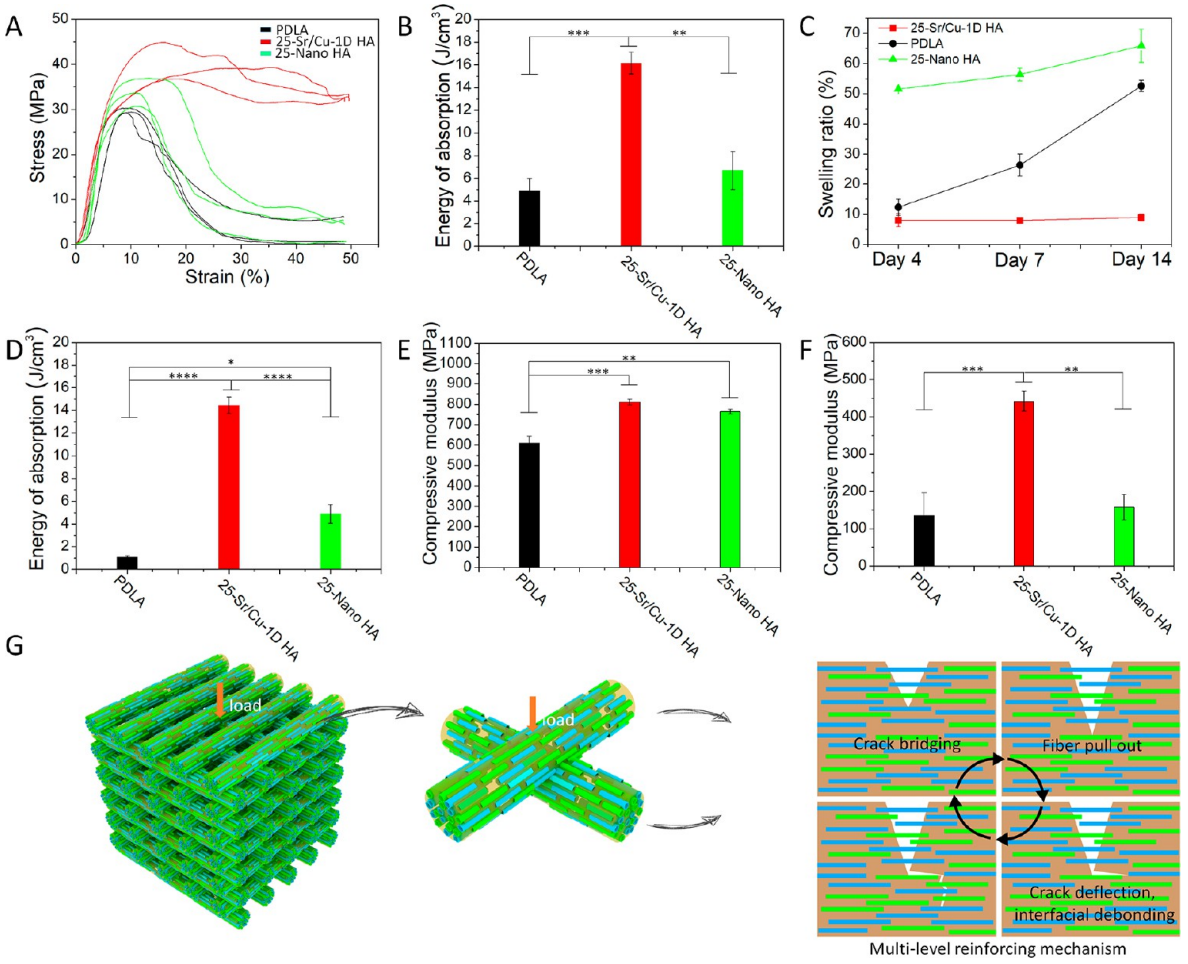

Figure 7. (A, B) Compressive stress−strain curves and energy of absorption per unit volume of the Sr/Cu-doped 1D HA/PDLA porous scaffolds, pure PDLA porous scaffolds, and Nano HA/PDLA porous scaffolds, respectively. (C) Swelling ratio of the Sr/Cu-doped 1D HA/PDLA porous scaffolds, pure PDLA porous scaffolds, and Nano HA/PDLA porous scaffolds in SBF at 37 °C for different time intervals (4, 7, and 14 days). (D) Energy of absorption per unit volume of the Sr/Cu-doped 1D HA/PDLA porous scaffolds, pure PDLA porous scaffolds, and Nano HA/PDLA porous scaffolds after a 14-day hMSC culture. (E, F) Compressive modulus of the pure PDLA porous scaffolds, Nano HA/PDLA porous scaffolds, and Sr/Cu-doped 1D HA/PDLA porous scaffolds before (E) and after (F) a 14-day hMSCs culture. (G) Schematic illustration of the proposed reinforcement mechanism of aligned Sr/Cu-doped 1D HA in the PDLA matrix. (*) for $p < 0.05$, (**) for $p < 0.01$, (***) for $p < 0.001$, and (****) for $p < 0.0001$.

PDLA and Nano HA/PDLA scaffolds, Sr/Cu-doped 1D HA/PDLA porous scaffolds exhibited a higher yield strength, which was retained at larger strain values, indicating that the scaffold did not collapse (Figure S9, Supporting Information). The energy of absorption per unit volume of the Sr/Cu-doped 1D HA/PDLA porous scaffolds was 3.3 times and 2.4 times higher than that of pure PDLA porous scaffolds and Nano HA/PDLA porous scaffolds, respectively (Figure 7B).

The superior structural stability of the Sr/Cu-doped 1D HA/PDLA porous scaffolds was further confirmed by a swelling test. The swelling behavior of the porous scaffolds in simulated body fluid (SBF) at 37 °C for the time intervals of 4, 7, and 14 days is shown in Figure 7C. The Sr/Cu-doped 1D HA/PDLA porous scaffolds had a controlled swelling behavior during the test. The Sr/Cu-doped 1D HA/PDLA porous scaffolds exhibited a swelling ratio of 8% at day 4, after which it remained stable up to day 14. In contrast, both pure PDLA porous scaffolds and Nano HA/PDLA porous scaffolds showed an increase in swelling ratio over the 14-day period. The swelling ratio of the pure PDLA porous scaffolds increased from 12.3% at day 4 to 52.6% at day 14. Nano HA/PDLA porous scaffolds had the highest swelling ratio at day 4, which was as high as 51.5%, and then increased to 65.9% at day 14. On the one hand, the presence of Nano HA increased the hydrophilicity of the composite.[52] On the other hand, Nano HA has a relatively limited ability to constrain the swelling of the PDLA matrix compared to Sr/Cu-doped 1D HA. Therefore, the swelling ratio of Nano HA/PDLA porous scaffolds at day 4 was high relative to the other groups. A pronounced increase in swelling ratio due to the incorporation of Nano HA into a PLA-based matrix was also observed in other studies.[53−55]

To study the long-term structural stability and mechanical properties of the materials upon exposure to a physiologically relevant environment, the porous scaffolds of Sr/Cu-doped 1D HA/PDLA and the Nano HA/PDLA and pure PDLA controls were exposed to a compressive test after a 14-day culture of hMSCs (Figure S10, A to C, Supporting Information). As can be seen from the compressive stress−strain curves of the scaffolds before and after cell culture, pure PDLA and Nano HA/PDLA porous scaffolds showed a strong decrease in mechanical properties following cell culture (Figure S10, A and

https://doi.org/10.1021/acsnano.1c03905
ACS Nano 2021, 15, 17480−17498

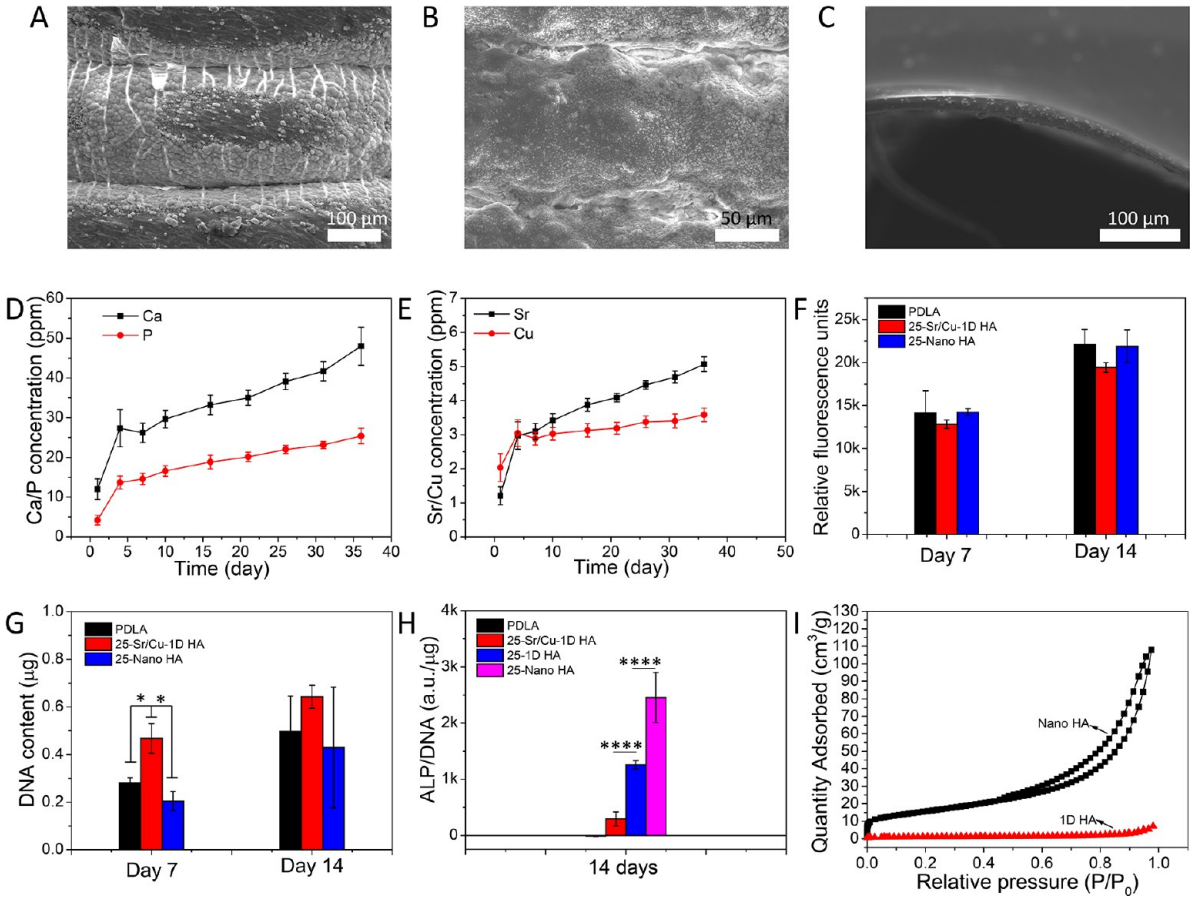

Figure 8. (A–C) *In vitro* mineralization of Sr/Cu-doped 1D HA/PDLA porous scaffolds (A), Nano HA/PDLA porous scaffolds (B), and pure PDLA porous scaffolds (C) in SBF at 37 °C for 7 days. (D) Cumulative amounts of Ca and P in physiological saline solution in time upon immersion of Sr/Cu-doped 1D HA/PDLA porous scaffolds. (E) Cumulative amounts of Sr and Cu in physiological saline solution in time upon immersion of Sr/Cu-doped 1D HA/PDLA porous scaffolds. (F, G) Metabolic activity and DNA content of hMSCs cultured for 7 and 14 days on pure PDLA porous scaffolds, Nano HA/PDLA porous scaffolds, and Sr/Cu-doped 1D HA/PDLA porous scaffolds. (H) ALP activity of hMSCs cultured for 14 days on pure PDLA porous scaffolds, Sr/Cu-doped 1D HA/PDLA porous scaffolds, undoped 1D HA/PDLA porous scaffolds, and Nano HA/PDLA porous scaffolds, respectively. (I) N_2 adsorption–desorption isotherms of Nano HA and undoped 1D HA. (*) for $p < 0.05$, (**) for $p < 0.01$, (***) for $p < 0.001$, and (****) for $p < 0.0001$.

B, Supporting Information), while the Sr/Cu-doped 1D HA/PDLA porous scaffolds still showed a relatively high compressive strength (Figure S10C, Supporting Information). The energy of absorption per unit volume during the compressive test of the Sr/Cu-doped 1D HA/PDLA porous scaffolds after cell culture was 13.4 times and 2.96 times higher than that of pure PDLA and Nano HA/PDLA porous scaffolds, respectively (Figure 7D).

The compressive modulus of the Sr/Cu-doped 1D HA/PDLA porous scaffolds before cell culture was comparable to that of Nano HA/PDLA and slightly higher than that of pure PDLA (Figure 7E). However, after a 14-day cell culture, the compressive modulus of the Sr/Cu-doped 1D HA/PDLA porous scaffolds was significantly higher than that of pure PDLA (3.3 times) and of Nano HA/PDLA (2.8 times) (Figure 7F).

As discussed earlier, the excellent mechanical strength and toughness of natural bone are attributed to its biphasic, hierarchical, and anisotropic structure. The highly aligned collagen fibers and HA crystals toughen bone by multiple toughing mechanisms including fibrillar sliding, crack bridging, and crack deflection.[56] Similar to the result of the tensile test in Figure 5E, it is suggested (and illustrated in Figure 7G) that the resistance to swelling and retention of compressive strength and toughness of the Sr/Cu-doped 1D HA/PDLA porous scaffold upon exposure to cells and cell culture medium can be attributed to its bone-like microstructure and analogous toughening mechanisms, resulting from aligned Sr/Cu-doped 1D HA fibers, which have strong interfacial interactions with the PDLA matrix, such as through hydrogen bonds.[57]

***In Vitro* Mineralization, Ion Release, and Bioactivity of Sr/Cu-Doped 1D HA/PDLA Porous Scaffolds.** In bone regeneration, the ability of a biomaterial to facilitate deposition of (bone) mineral on its surface is considered an important bioactivity characteristic. One way of investigating this characteristic *in vitro* is by immersing the material in SBF and studying the process of mineral formation on its surface.[58] The results of an *in vitro* mineralization test of the biomimetic Sr/Cu-doped 1D HA/PDLA porous scaffolds, in comparison with pure PDLA and Nano HA/PDLA porous scaffolds with the same amount of HA, are shown in Figure 8. After incubation in SBF at 37 °C for 7 days, numerous mineralized spots were observed on the Sr/Cu-doped 1D HA/PDLA porous scaffold and the Nano HA/PDLA porous scaffolds (Figure 8, A and B), but only sparse mineralized clusters formed on the pure PDLA porous scaffolds (Figure 8C). The

https://doi.org/10.1021/acsnano.1c03905
ACS Nano 2021, 15, 17480–17498

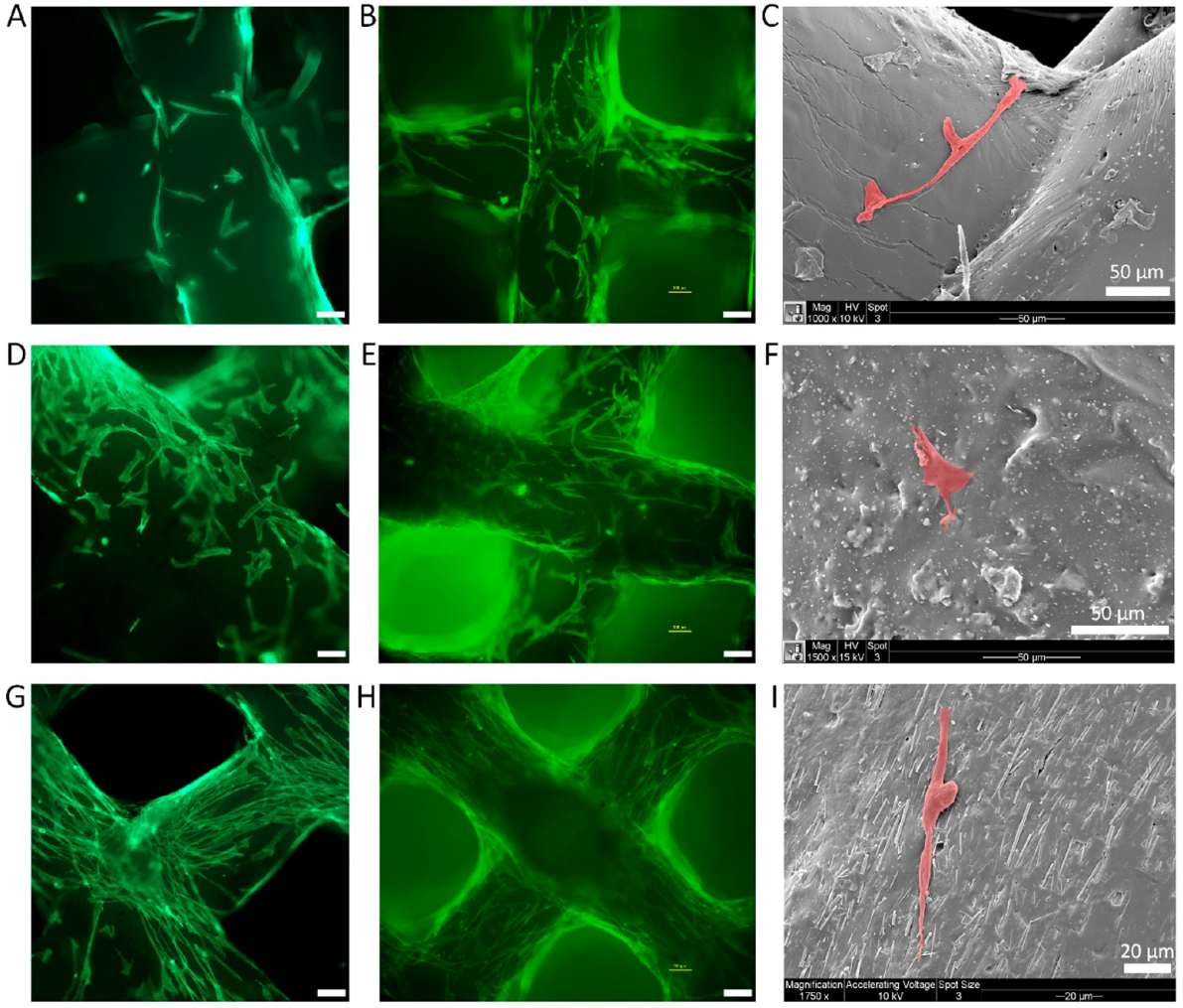

Figure 9. (A, B) Fluorescence microscopy images of actin cytoskeleton (phalloidin: green) staining of hMSCs cultured on pure PDLA porous scaffolds for 3 and 7 days, respectively. (C) SEM micrographs of hMSCs cultured on pure PDLA porous scaffolds for 3 days. (D, E) Fluorescence microscopy images of actin cytoskeleton (phalloidin: green) staining of hMSCs cultured on Nano HA/PDLA porous scaffolds for 3 and 7 days, respectively. (F) SEM micrographs of hMSCs cultured on Nano HA/PDLA porous scaffolds for 3 days. (G, H) Fluorescence microscopy images of actin cytoskeleton (phalloidin: green) staining of hMSCs cultured on Sr/Cu-doped 1D HA/PDLA porous scaffolds for 3 and 7 days, respectively. (I) SEM micrographs of hMSCs cultured on Sr/Cu-doped 1D HA/PDLA porous scaffolds for 3 days. Unlabeled scale bar: 100 μm.

improvement of the *in vitro* mineralization ability of polymers by incorporating HA has been reported in other studies.[59−61]

The release profiles of calcium (Ca), inorganic phosphate (P), Sr, and Cu ions from Sr/Cu-doped 1D HA/PDLA porous scaffolds upon immersion in a physiological saline solution are shown in Figure 8, D and E. While various solutions have been used *in vitro* to study degradation of and the release profile of (inorganic) constituents and additives from biomaterials including PBS,[62] SBF,[63] and cell culture medium,[64] here we selected a physiological saline solution for its simple composition compared to other solutions and the fact that it initially does not contain Ca or P ions. The Sr/Cu-doped 1D HA/PDLA porous scaffolds exhibited a relatively rapid Ca, P, Sr, and Cu ion release during the initial 4 days, followed by leveling-off and a more sustained release until day 36. According to the literature, in the context of bone regeneration the Cu ion acts as a double-edged sword; depending on the concentration, Cu ions have been shown to enhance angiogenesis, but also to induce cell death.[65] In the biomimetic Sr/Cu-doped 1D HA/PDLA porous scaffolds developed here, the amount of Sr/Cu-doped 1D HA was 25 wt %, which in turn consisted of 1D Sr-HA and 1D Cu-HA in a 1:1 ratio. A preliminary live/dead assay with hMSCs cultured on these scaffolds (Figure S11, Supporting Information) showed a large number of dead cells, suggesting that the amount of Cu ions within the scaffolds may have been too high (Cu/Ca × 100% = 2.5% in total, mole ratio). Therefore, for the following experiments, we changed the ratio of the 1D Sr-HA/1D Cu-HA from 50 wt %/50 wt % to 80 wt %/20 wt % while maintaining the total amount of Sr/Cu-doped 1D HA at 25 wt %.

hMSCs cultured on these scaffolds showed an increase in metabolic activity as well as DNA content over a culture period of 14 days (Figure 8, F and G), indicating that the cells were able to proliferate on the Sr/Cu-doped 1D HA/PDLA porous scaffolds. No significant differences were observed in metabolic activity among biomimetic Sr/Cu-doped 1D HA/PDLA, Nano HA/PDLA, and pure PDLA porous scaffolds at either time point. Similarly, the DNA amount was comparable at 14 days, while at 7 days, Sr/Cu-doped 1D HA/PDLA scaffolds showed

https://doi.org/10.1021/acsnano.1c03905
ACS Nano 2021, 15, 17480−17498

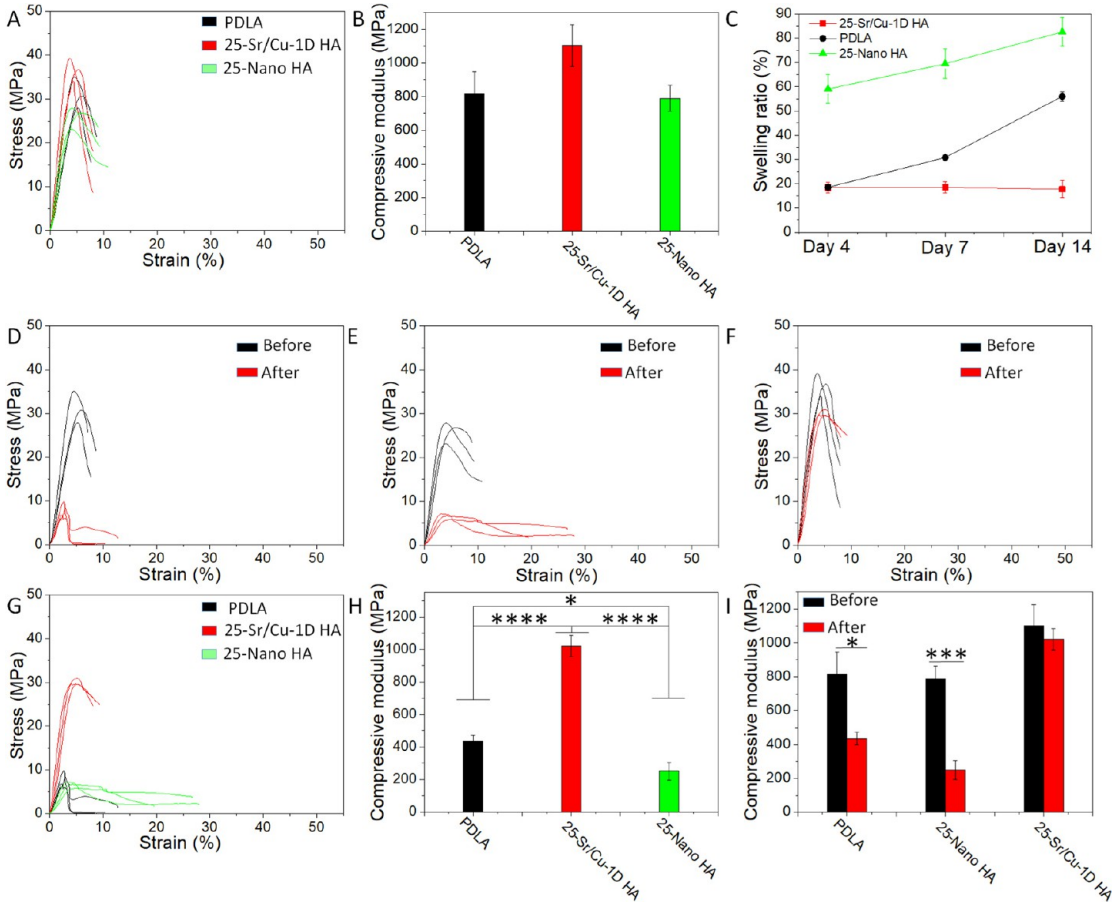

Figure 10. (A, B) Compressive stress−strain curves and compressive modulus of the assembled Sr/Cu-doped 1D HA/PDLA porous scaffolds, assembled PDLA porous scaffolds, and assembled Nano HA/PDLA porous scaffolds, respectively. (C) Swelling ratio of the assembled Sr/Cu-doped 1D HA/PDLA porous scaffolds, assembled PDLA porous scaffolds, and assembled Nano HA/PDLA porous scaffolds in SBF at 37 °C for different time intervals (4, 7, and 14 days). (D−F) Compressive stress−strain curves of the assembled PDLA porous scaffolds (D), assembled Nano HA/PDLA porous scaffolds (E), and assembled Sr/Cu-doped 1D HA/PDLA porous scaffolds (F) before and after a 14-day hMSC culture. (G, H) Compressive stress−strain curves and compressive modulus of the assembled Sr/Cu-doped 1D HA/PDLA porous scaffolds, assembled PDLA porous scaffolds, and assembled Nano HA/PDLA porous scaffolds after a 14-day hMSC culture. (I) Compressive modulus of the assembled PDLA porous scaffolds, assembled Nano HA/PDLA porous scaffolds, and assembled Sr/Cu-doped 1D HA/PDLA porous scaffolds before and after a 14-day hMSC culture. (*) for $p < 0.05$, (**) for $p < 0.01$, (***) for $p < 0.001$, and (****) for $p < 0.0001$.

a significantly higher DNA amount than Nano HA/PDLA and PDLA porous scaffolds. Therefore, the Sr/Cu-doped 1D HA/PDLA porous scaffolds showed a good biocompatibility.

Additionally, we tested the ability of the material to support the alkaline phosphatase (ALP) enzymatic activity of hMSCs, which is an early marker of osteogenic differentiation (Figure 8H). While all composite scaffolds showed a higher ALP activity than pure PDLA scaffolds, the ALP expression of hMSCs cultured on the Sr/Cu-doped 1D HA/PDLA porous scaffolds was lower than that of undoped 1D HA/PDLA porous scaffolds, suggesting that the presence of Sr and Cu ions decreased the ALP activity of cells. Previous work suggested a beneficial effect of cosubstitution of Sr and Cu ions on the ALP activity;[66,67] however, due to differences in the biomaterial used as well as cell types tested, a direct comparison with our study is difficult to make. The high ALP activity by hMSCs grown on Nano HA/PDLA might be attributed to the nanoscale dimension of Nano HA used for the preparation of the composite. Nano HA had a significantly higher specific surface area (56.08 m^2/g) than the microsized 1D HA crystals (3.64 m^2/g) (Figure 8I). Therefore, it is suggested that the surface exposure of the Nano HA to hMSCs was more pronounced, resulting in a positive effect on the ALP activity of hMSCs. Previous studies have shown the beneficial effects of smaller-size HA particles (20−100 nm) on the expression of osteoblast-related markers by bone marrow MSCs than similar particles with a larger size (150−250 nm).[68,69]

Taken together, these results showed that the Sr/Cu-doped 1D HA/PDLA composite supported proliferation and ALP activity, a marker of osteogenic differentiation of hMSCs, enhancing it relative to pure PDLA porous scaffolds. Further research is needed to study specific effects of Cu, Sr, or other ions that can be incorporated into the 1D HA ceramic on the osteogenic differentiation of MSCs on both protein and gene expression level, which was beyond the aim of this study.

After 3 and 7 days of culture, the morphology of hMSCs on the Sr/Cu-doped 1D HA/PDLA, Nano HA/PDLA, and PDLA porous scaffolds was observed by using fluorescence microscopy and SEM (Figure 9; Figure S12, Supporting Information). On PDLA porous scaffolds, the cells were observed on the scaffold fibers and exhibited random

https://doi.org/10.1021/acsnano.1c03905
ACS Nano 2021, 15, 17480−17498

morphology (Figure 9, A to C). Similarly, hMSCs cultured on the Nano HA/PDLA porous scaffold showed a random morphology (Figure 9, D to F). Moreover, visually, more cells were present on Nano HA/PDLA than on pure PDLA scaffolds, suggesting that the presence of Nano HA enhanced the attachment of cells but did not affect their orientation. Interestingly, on the Sr/Cu-doped 1D HA/PDLA porous scaffolds, the cells exhibited an elongated morphology and were orientated in the direction of the alignment of Sr/Cu-doped 1D HA crystals in the composite (Figure 9, G to I). Differences in not only chemical but consequently also physical properties between HA and PDLA, including wettability, surface charge, and surface structural properties, may be a reason for preferential cell attachment to the ceramic phase. The elongation and orientation of the cells is attributed to contact guidance by the anisotropic 1D HA crystals, which will be discussed in greater detail in the next section. Taken together, the morphology analyses suggested that the presence of Sr/Cu-doped 1D HA not only enhanced attachment of the hMSCs, but also directed their morphology and orientation.

Collagenous Matrix Deposition on Sr/Cu-Doped 1D HA/PDLA Porous Scaffolds. While the effect of structural organization of the organic and inorganic components of bone on the mechanical properties is well understood, the influence of collagen fiber and HA crystal orientation in bone tissue on the regulation of cellular processes has not been fully understood so far.[70] In the human body, osteocyte morphology is dependent on the type of bone tissue. Elongated osteocytes are found in load-bearing long bones that are predominantly loaded parallel to their longitudinal direction.[71] Osteocyte lacunae are aligned to the collagen fiber orientation, and the formation of a highly oriented collagen matrix may require an alignment of osteoblasts.[72] A promising approach to mimic the bone cell−bone matrix interactions is the use of nano- or micropatterned substrates, which can provide directional cues in regulating cell behavior and collagen matrix assembly and alignment in a preferred direction.[70,73] Nevertheless, these patterning approaches are often restricted to the two-dimensional (2D) level and cannot be easily translated to 3D bone graft substitutes.

As discussed so far, the porous scaffolds were built using fiber deposition in the 0−90 deg direction. As a consequence, not all fibers in the scaffold had the same orientation of Sr/Cu-doped 1D HA crystals. Therefore, in order to investigate whether the physical properties of the scaffold could be further improved by ensuring the same orientation of the ceramic phase throughout the scaffold, and how this influences the cell behavior, a Sr/Cu-doped 1D HA/PDLA porous scaffold with all the Sr/Cu-doped 1D HA aligned in the longitudinal direction was developed by using 3D printing followed by manual assembly. Moreover, these assembled scaffolds were used to investigate whether the observed effect of Sr/Cu-doped 1D HA/PDLA porous scaffolds on the alignment and orientation of hMSCs also translates to the modified properties of the ECM secreted by cells. The fabrication process of the assembled Sr/Cu-doped 1D HA/PDLA porous scaffold is shown in Figure S13. Two types of building blocks were prepared by layer-by-layer printing in the 0−0 deg direction. Then, the building blocks were assembled into 3D porous scaffolds manually. During the assembly process, one side of the building block (labeled in red in Figure S13A, Supporting Information) was wetted by acetone by putting it on a piece of paper that was soaked with acetone beforehand for 10 s. Subsequently, the building blocks were stacked on the top of each other to form a 3D porous scaffold. The alignment of Sr/Cu-doped 1D HA in the building blocks was characterized by SEM. As shown in Figure S13, B to D (Supporting Information), all the Sr/Cu-doped 1D HA were aligned in the longitudinal direction.

The mechanical properties of the assembled Sr/Cu-doped 1D HA/PDLA porous scaffolds with a porosity of 50% are shown in Figure 10. Assembled PDLA porous scaffolds and assembled Nano HA/PDLA porous scaffolds with the same porosity were used as controls. The assembled Sr/Cu-doped 1D HA/PDLA porous scaffolds again showed higher values for compressive strength, Young's modulus, swelling resistance, and long-term structural stability compared to the controls. The highest compressive strength of the assembled Sr/Cu-doped 1D HA/PDLA porous scaffolds was around 36.6 MPa (Figure 10A). The compressive modulus of the assembled Sr/Cu-doped 1D HA/PDLA porous scaffolds was as high as 1.1 GPa (Figure 10B), which was higher, although not statistically significant, than that of the controls as well as that of the fully printed porous scaffolds with the same porosity described above. The reason that the modulus of the assembled porous scaffolds was higher than that of the fully printed porous scaffolds is plausibly related to the fact that in the assembled scaffold all Sr/Cu-doped 1D HA/PDLA crystals were oriented in the same direction, thus active in supporting the load (Figure S14A, Supporting Information). In contrast, in the fully printed Sr/Cu-doped 1D HA/PDLA porous scaffolds, the Sr/Cu-doped 1D HA aligned in the transversal direction in the composite (Figure S14B, Supporting Information) were less effective in supporting the load.

Similar to the fully printed Sr/Cu-doped 1D HA/PDLA porous scaffolds, the assembled Sr/Cu-doped 1D HA/PDLA porous scaffolds showed controlled swelling behavior, although the swelling ratio was higher, up to 18% compared to the 8% observed for the fully 3D printed scaffolds (Figure 10C). Also this affect can be attributed to the fact that in the assembled composite, where all 1D HA crystals were oriented in the same direction, swelling of the composite was effectively constrained in the *z*-direction, whereas in the fully printed scaffolds, this effect occurred in two directions. Moreover, the pore walls of the assembled scaffold were compact, whereas in the fully printed scaffold, space among the fibers could consume part of the swelling. Therefore, the fully printed Sr/Cu-doped 1D HA/PDLA porous scaffolds as well as the fully printed PDLA and Nano HA/PDLA porous scaffolds showed a lower swelling ratio compared to that of the assembled ones.

The assembled Sr/Cu-doped 1D HA/PDLA porous scaffolds possessed superior structural stability. After a 14-day hMSC culture, the compressive strength of the assembled PDLA (Figure 10D) and assembled Nano HA/PDLA porous scaffolds (Figure 10E) showed a strong decrease. However, the highest compressive strength of the assembled Sr/Cu-doped 1D HA/PDLA porous scaffolds was still as high as 30.1 MPa (Figure 10F), which was more than 3 times higher than that of the controls (Figure 10G). The compressive modulus of the assembled Sr/Cu-doped 1D HA/PDLA porous scaffolds after *in vitro* cell culture was 1.02 GPa (Figure 10H) and comparable to the modulus before the cell culture (Figure 10I). In contrast, the compressive modulus of the assembled PDLA and Nano HA/PDLA porous scaffolds decreased by 46.7% and 68.3%, respectively (Figure 10, H and I). Taken together, by assembling printed fibers in such a way that all

https://doi.org/10.1021/acsnano.1c03905
ACS Nano 2021, 15, 17480−17498

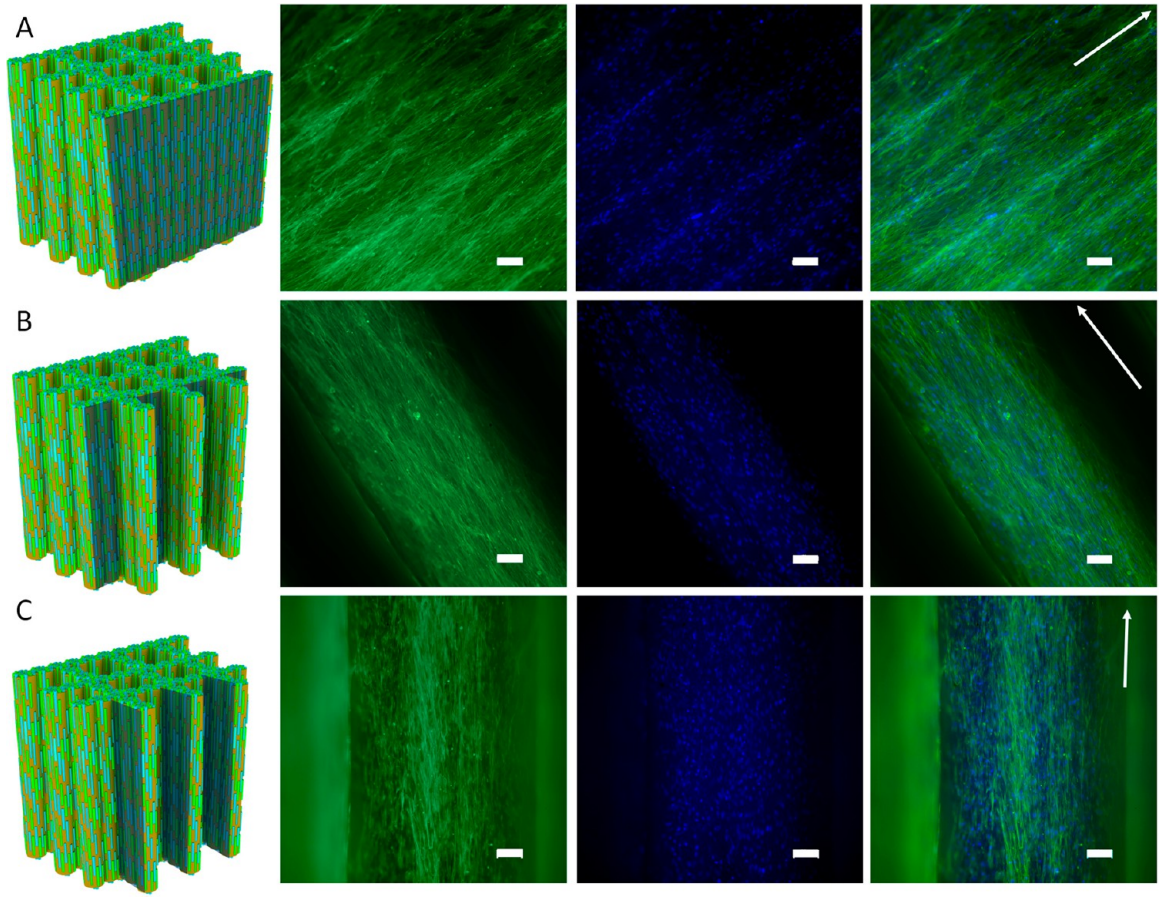

Figure 11. (A–C) Fluorescence microscopy images of actin cytoskeleton (phalloidin: green) and nuclei (DAPI: blue) staining of hMSCs cultured on the assembled Sr/Cu-doped 1D HA/PDLA porous scaffolds for 4 days. Arrows indicate the direction of the ceramic alignment. Scale bar: 100 μm.

ceramic crystals inside the porous scaffold were aligned in the same direction, further improvement of the mechanical properties was achieved.

Next, the morphology of hMSCs after 4 days of culture on the assembled Sr/Cu-doped 1D HA/PDLA porous scaffolds and assembled Nano HA/PDLA porous scaffolds was studied using fluorescence staining of the actin cytoskeleton and nuclei. As expected, the cells exhibited an elongated morphology and were oriented in the direction of the ceramic phase. Because of the scaffold design, the orientation of hMSCs was the same on the scaffold periphery and on the pore walls (Figure 11, A to C). In contrast, the hMSCs seeded on the assembled Nano HA/PDLA porous scaffolds exhibited different behavior. The cells on the scaffold periphery were randomly oriented (Figure S15A, Supporting Information), in contrast to the cells on the periphery of the assembled Sr/Cu-doped 1D HA/PDLA porous scaffolds (Figure 11A). However, the hMSCs on the pore walls of the assembled Nano HA/PDLA porous scaffolds showed preferred orientation in the longitudinal direction (Figure S15, B and C, Supporting Information) despite the fact that Nano HA particles were randomly distributed inside the composite. A reason for this may be the limited space in the transversal direction, leading to cells attaching in the longitudinal direction of the fibers.

At day 14, the morphology of hMSCs and type I collagen, a component of the secreted extracellular matrix (ECM), was visualized by immunofluorescence staining. As shown in Figure 12, A to C, throughout the assembled Sr/Cu-doped 1D HA/PDLA porous scaffolds, both actin and type I collagen were aligned in the direction of Sr/Cu-doped 1D HA crystals. For the assembled Nano HA/PDLA porous scaffolds, random actin and type I collagen were found on the scaffold periphery, while the cells and ECM were aligned on the pore walls (Figure S16, A to C, Supporting Information). These results demonstrate that the morphology and orientation of not only the cells but also of the ECM produced by the cells were directed by the structural properties of the scaffold, and more specifically, the orientation of Cu/Sr-doped 1D HA crystals, although the available scaffold area for cell attachment also played a role. Previous studies have shown that topographical cues, derived from surface-patterning of biomaterial surfaces, influenced cytoskeletal morphology and orientation of focal adhesions. The contact guidance provided by nano- and/or microtopographical features affected hMSC adhesion, migration, and even proliferation and differentiation.[74−78] Moreover, hMSCs' directional migration and ECM remodeling under the influence of topographical stimuli at the micro- and nanoscale have been investigated on various substrates.[79−82] Cells organize and interact with ECM through integrins, guided by different stimuli, to generate patterns, essential for tissue and organ functions. Reciprocally, the ECM influences the morphology and phenotype *via* bidirectional integrin signaling.[83,84] Based on this body of evidence, it is reasonable to suggest that also in the biomimetic Sr/Cu-doped 1D HA/PDLA porous scaffolds developed here, integrin signaling plays

https://doi.org/10.1021/acsnano.1c03905
ACS Nano 2021, 15, 17480−17498

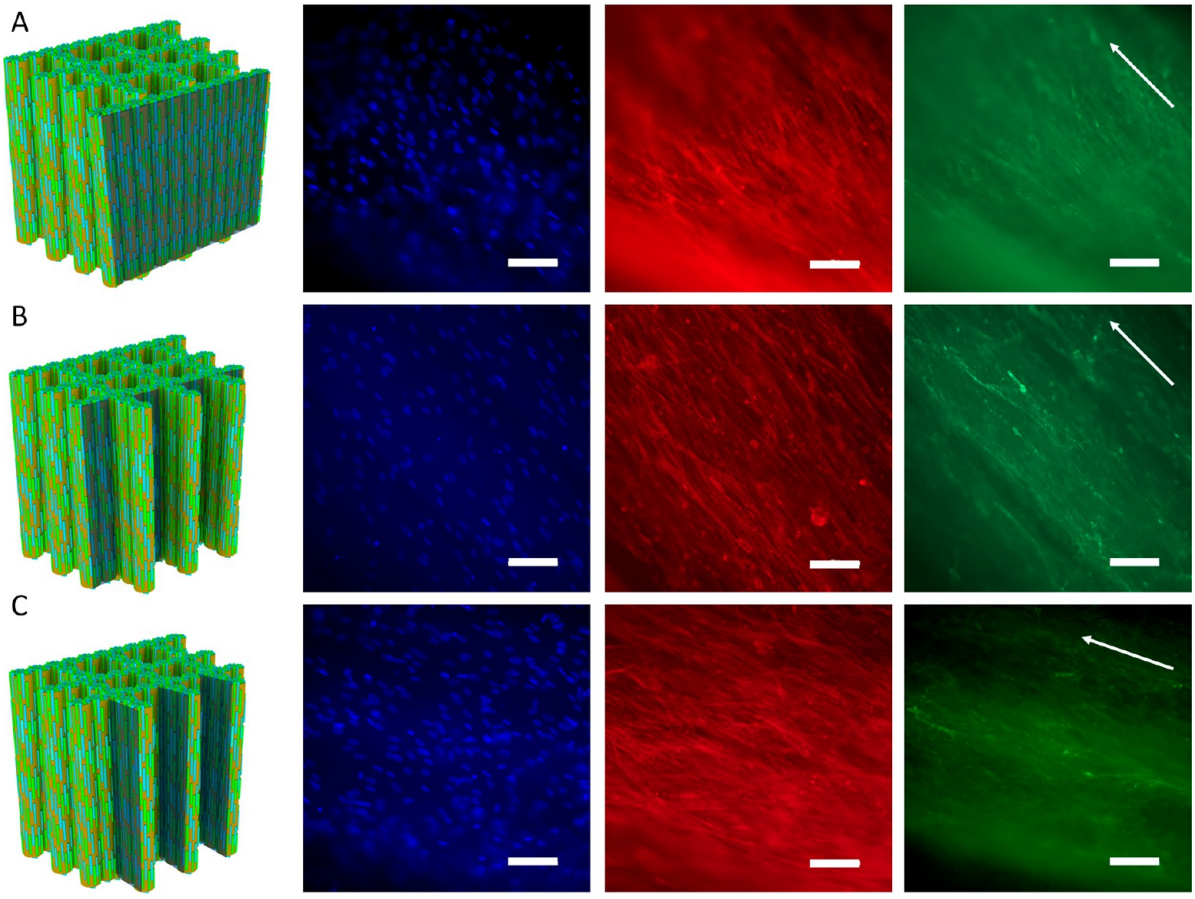

Figure 12. (A–C) Fluorescence microscopy images of nuclei (DAPI: blue), actin cytoskeleton (phalloidin: red), and type I collagen (green) of hMSCs cultured on the assembled Sr/Cu-doped 1D HA/PDLA porous scaffolds for 14 days. Arrows indicate the direction of the ceramic alignment. Scale bar: 100 μm.

a role in hMSC organization and directional collagen matrix formation, in 3D.

In sum, by using the Sr/Cu-doped 1D HA for developing anisotropic porous composite scaffolds, we succeeded in significantly improving the mechanical properties and also controlling the orientation of hMSCs and the formation of anisotropic bone-like type I collagen in 3D. In other words, the Sr/Cu-doped 1D HA/PDLA scaffolds mimicked not only the microstructure, and hence the mechanical properties of natural bone, but also the function of the bone matrix in modulating the cell behavior. Therefore, the biomimetic Sr/Cu-doped 1D HA/PDLA composites developed here may serve as a 3D platform for the investigation of how the bone matrix regulates of the orientation of cells and the property of the ECM secreted by these cells in bone tissue.

CONCLUSION

In this work, inspired by the composition and microstructure of natural bone, a biomimetic, biphasic composite consisting of PDLA as an organic matrix and uniformly dispersed, highly aligned Sr/Cu-doped 1D HA as an inorganic reinforcement phase was developed. The presence and alignment of Sr/Cu-doped 1D HA crystals resulted in mechanical reinforcement of the polymer matrix, including compressive and tensile strength, compressive modulus, and fracture toughness, making them comparable to the mechanical properties of cortical bone. Moreover, the interfacial interactions between the polymer matrix and aligned anisotropic ceramic crystals endowed the composite with pronounced swelling resistance and long-term structural and mechanical stability upon exposure to a physiological environment. Sr and Cu ions substituted into 1D HA could be sustainably released from the composite. Moreover, the composite facilitated mineral deposition from SBF and supported attachment, proliferation, and ALP activity of hMSCs. Finally, the highly aligned Sr/Cu-doped 1D HA crystals in the composite induced the alignment of hMSCs and formation of anisotropic collagen fiber matrix. The method and design principles applied here may provide inspiration for the development of advanced composites for bone regeneration with improved mechanical properties and bioactivity. Moreover, the biomimetic composite may serve as a 3D platform for studying cell–ECM interactions in bone tissue.

EXPERIMENTAL SECTION

Sr/Cu-Doped 1D HA/PCL Filament Preparation. The initial feasibility experiments aimed at producing aligned ceramic/polymer composite filaments were performed using PCL as a model polymer. PCL is approved by the Food and Drug Administration (FDA) for biomedical applications and has been extensively studied for fabrication of synthetic bone graft substitutes. The reason that we chose PCL in this part is its relatively low cost compared to other biopolymers. The typical procedure for preparation of Sr/Cu-doped 1D HA/PCL filaments was as follows: 5 g of 1D Sr-HA and 5 g of 1D Cu-HA were added to 50 mL of chloroform in a glass bottle at room temperature and stirred for 2 h using a magnetic stirrer. The weights of the glass bottle and the magnetic stir bar were measured. Then, 10 g of PCL was added to the solution followed by continuous stirring,

https://doi.org/10.1021/acsnano.1c03905
ACS Nano 2021, 15, 17480–17498

allowing chloroform to evaporate, and the weight of the total system was measured until the concentration of the solid content reached 33 wt %. Subsequently, the solution was loaded in a syringe and extruded through a needle at the desired speed under the control of a syringe pump (ProSense B.V. NE-300, USA). To investigate the effect of the extrusion rate, the diameter and length of the needle, and the concentration of the solid content on the structure of the extruded filaments, three different extrusion rates (100, 200, 400 μL/min), three needles with the same length (10 mm) but different diameters (18G, 21G, 25G), three needles with the same diameter (21G) but different lengths (2, 6, 10 mm), and three suspensions with different concentration of the solid content (24.42, 33.33, 42.24 wt %) were tested. Finally, Sr/Cu-doped 1D HA/PCL filaments fabricated under different conditions were immersed in liquid nitrogen and broken into small pieces. These small samples were sputtered with gold, and their cross-sections were observed using an SEM (Philips XL30, The Netherlands).

Sr/Cu-Doped 1D HA/PCL Compact Sample Preparation. In order to investigate how the mass ratio between HA and PCL influences the mechanical properties, we prepared Sr/Cu-doped 1D HA/PCL compact samples with different amounts of Sr/Cu-doped 1D HA (0, 10, 30, 50 wt %). Unless stated otherwise, the Sr/Cu-doped 1D HA is a mixture of 1D Sr-HA (50 wt %) and 1D Cu-HA (50 wt %). Typically, solutions consisting of Sr/Cu-doped 1D HA/PCL (33 wt %) and chloroform (67 wt %) with different amounts of Sr/Cu-doped 1D HA were prepared. Sr/Cu-doped 1D HA/PCL compact composites with desired dimensions were made by extruding the solutions through a nozzle (24G) by using a 3D plotting system (Bioplotter, Japan). The moving speed of the plotting head was set at 4 mm s^{-1}, and the pressure was 5 bar. All samples were prepared by layer-by-layer printing of the solutions in the 0−0 deg direction. The displacement of the printer head for printing adjacent fibers in the x−y plane was set at 0.13 mm. Similarly, the displacement of the printer head during printing different layers in the z direction was set at 0.12 mm; 0.12 mm is smaller than the diameter of the nozzle (24G, 0.3 mm), thus ensuring that the printed composite was compact. The composites were dried in a fume hood until a constant weight was obtained. Moreover, to compare the mechanical reinforcement performance between Sr/Cu-doped 1D HA used in this work and conventional nanosized HA powder (Nano HA), Nano HA/PCL compact composites with 30 and 50 wt % of ceramic phase were also fabricated under the same conditions.

Mechanical Properties of Sr/Cu-Doped 1D HA/PCL Compact Samples. Compressive and tensile tests were performed on an ElectroForce 3200 machine (ElectroForce 3200, USA), with a 450 N load cell. For the tensile test, three rectangular specimens with dimensions of 60 × 5 × 1 mm^3 were tested at a rate of 9 mm min^{-1}. The samples were fixed on the mechanical testing machine by using two clamps on both ends of the sample. A piece of sandpaper was placed between the sample and the clamp on each side to avoid sample sliding during the test. For compressive tests, three specimens with dimensions of 3 × 3 × 4 mm^3 were tested at a rate of 0.5 mm min^{-1}. For both tests, pure PCL samples and Nano HA/PCL samples with the same dimensions as the experimental samples were used as controls. Young's modulus, or the modulus of elasticity, was defined as the slope of the linear region of the stress−strain curve.

Sr/Cu-Doped 1D HA/PDLA Compact Samples and Porous Scaffold Preparation. A 2.5 g amount of 1D Sr-HA and 2.5 g of 1D Cu-HA were added into 30 mL of acetone at room temperature and mixed using a magnetic stirrer for 2 h. Then 15 g of PDLA was added to the solution and mixed until the acetone evaporated, resulting in a mixture of Sr/Cu-doped 1D HA (25 wt %) and PDLA (75 wt %). The remaining mixture of Sr/Cu-doped 1D HA and PDLA was further dried in a vacuum oven at 30 °C for 3 days. Sr/Cu-doped 1D HA/PDLA compact composites and porous scaffolds with desired shapes were made by extruding the mixture of Sr/Cu-doped 1D HA and PDLA through a nozzle (23G) at 145 °C by using a 3D plotting system (Bioplotter, Japan). The moving speed of the plotting head was 4 mm s^{-1}, and the pressure was 5 bar. Compact composite samples were prepared by layer-by-layer printing in 0−0 deg direction. The displacement of the printer head for printing adjacent fibers in the x−y plane, as well as for printing different layers in the z direction, was set at 0.2 mm, ensuring deposition of compact samples. Sr/Cu-doped 1D HA/PDLA porous scaffolds were prepared by layer-by-layer printing in the 0−90 deg direction. The displacement of the printer head for printing adjacent fibers in the x−y plane was set at 1 mm, and the displacement of the printer head for printing different layers in the z-direction was set at 0.1 mm. PDLA compact samples and porous scaffolds were prepared by using the same 3D plotting system and plotting parameters, at a temperature of 140 °C. Nano HA/PDLA compact samples and porous scaffolds with 25 wt % of Nano HA were also fabricated under the same conditions as the Sr/Cu-doped 1D HA/PDLA samples.

The porosity of the porous scaffolds was calculated by the following equation:

$$\text{Porosity} = (1 - \rho_1/\rho_2) \times 100\% \quad (1)$$

$$\rho_1 = M_1/V_1 \quad (2)$$

$$\rho_2 = (\rho_{HA}\rho_{PDLA})/(W_2\rho_{HA} + W_1\rho_{PDLA}) \quad (3)$$

where M_1 and V_1 are the mass and volume of the porous scaffolds, respectively. ρ_{HA} represents the theoretical density of HA, which is 3.16 g cm^{-3}, and ρ_{PDLA} represents the theoretical density of PDLA, which is 1.25 g cm^{-3}. W_1 and W_2 are the mass fraction of HA and PDLA in the porous scaffolds, respectively.

Mechanical Properties of Sr/Cu-Doped 1D HA/PDLA Compact Samples and Porous Scaffolds. Tensile tests were performed on an ElectroForce 3200 machine (ElectroForce 3200, USA), with a 450 N load cell. For tensile tests, three specimens with dimensions of 50 × 2.5 × 1 mm^3 were tested at a rate of 1 mm min^{-1}. Compressive tests were performed on a material testing machine (Zwick/Roell, Germany), with a 10 000 N load cell. For compressive tests, three specimens of compact composites with dimensions of 4 × 4 × 5 mm^3 and three specimens of porous scaffolds (50% porosity) with dimensions of 6 × 6 × 6 mm^3 were tested at a rate of 1 mm min^{-1}. Pure PDLA samples and Nano HA/PDLA samples with the same dimensions and porosity were used as controls. Young's modulus was calculated as described for the Sr/Cu-doped 1D HA/PCL samples above. Energy of absorption per unit volume (toughness) was calculated by integrating the area between the x-axis and the stress−strain curves.

The fracture toughness (K_Q) of Sr/Cu-doped 1D HA/PDLA compact samples with dimensions of 5 × 10 × 50 mm^3 (n = 3) was characterized by the SENB test according to the ISO 13586 standard. Pure PDLA and the Nano HA/PDLA composite with the same amount of HA were used as controls. A 4.6 mm deep notch (radius of 0.4 mm) was milled into the specimens. Due to the brittleness of the samples, a razor-blade cut was made into the tip of the notch instead of tapping a crack. The three-point bending test was performed on a tensile tester (Zwick Z010) equipped with a 1000 N load cell. The diameter of rollers, test speed, and test temperature were 10 mm, 10 mm/min, and 20 °C, respectively. Fracture toughness was calculated from the data according to the following equation by using Matlab R2021a:

$$K_Q = f(a/w)\frac{F_Q}{h\sqrt{w}} \quad (4)$$

where F_Q is the load at crack growth initiation, h is the test specimen thickness, w is the test specimen width, and $f(a/w)$ is the geometry calibration factor.

ASSOCIATED CONTENT

Supporting Information

The Supporting Information is available free of charge at https://pubs.acs.org/doi/10.1021/acsnano.1c03905.

Additional details about the synthesis of stoichiometric 1D HA, 1D Sr-HA, and 1D Cu-HA, swelling test, *in vitro*

https://doi.org/10.1021/acsnano.1c03905
ACS Nano 2021, 15, 17480−17498

mechanical stability test, *in vitro* mineralization test, *in vitro* ion release test, live/dead staining, metabolic activity test, quantification of DNA, ALP activity test, and collagen immunostaining (PDF)

AUTHOR INFORMATION

Corresponding Author

Pamela Habibovic − *Department of Instructive Biomaterials Engineering, Maastricht University, MERLN Institute for Technology-Inspired Regenerative Medicine, 6229 ER Maastricht, The Netherlands;* orcid.org/0000-0001-8249-5155; Email: p.habibovic@maastrichtuniversity.nl

Authors

Yonggang Zhang − *Department of Instructive Biomaterials Engineering, Maastricht University, MERLN Institute for Technology-Inspired Regenerative Medicine, 6229 ER Maastricht, The Netherlands*

Jiaping Li − *Department of Instructive Biomaterials Engineering and Complex Tissue Regeneration Department, Maastricht University, MERLN Institute for Technology-Inspired Regenerative Medicine, 6229 ER Maastricht, The Netherlands*

Vivian Hilda Maria Mouser − *Orthopaedic Biomechanics, Department of Biomedical Engineering, Eindhoven University of Technology, 5600 MB Eindhoven, The Netherlands*

Nadia Roumans − *Department of Cell Biology-Inspired Tissue Engineering, Maastricht University, MERLN Institute for Technology-Inspired Regenerative Medicine, 6229 ER Maastricht, The Netherlands*

Lorenzo Moroni − *Complex Tissue Regeneration Department, Maastricht University, MERLN Institute for Technology-Inspired Regenerative Medicine, 6229 ER Maastricht, The Netherlands;* orcid.org/0000-0003-1298-6025

Complete contact information is available at: https://pubs.acs.org/10.1021/acsnano.1c03905

Notes

The authors declare no competing financial interest.

ACKNOWLEDGMENTS

This research was financially supported by the Gravitation Program "Materials Driven Regeneration", funded by The Dutch Research Council NWO (Grant #024.003.013). JL, LM and PH acknowledge the financial support by the Dutch Research Council, Applied and Engineering Sciences NWO-AES (Grant #16711). The authors acknowledge Noah Avraham and Prof. Regina Palkovits (RWTH Aachen University, Germany) for assisting with BET measurement.

REFERENCES

(1) Bohner, M.; Miron, R. J. A Proposed Mechanism for Material-Induced Heterotopic Ossification. *Mater. Today* **2019**, *22*, 132−141.

(2) Wu, S. L.; Liu, X. M.; Yeung, K. W. K.; Liu, C. S.; Yang, X. J. Biomimetic Porous Scaffolds for Bone Tissue Engineering. *Mater. Sci. Eng., R* **2014**, *80*, 1−36.

(3) Woodruff, M. A.; Lange, C.; Reichert, J.; Berner, A.; Chen, F.; Fratzl, P.; Schantz, J.-T.; Hutmacher, D. W. Bone Tissue Engineering: From Bench to Bedside. *Mater. Today* **2012**, *15* (10), 430−435.

(4) Christy, P. N.; Basha, S. K.; Kumari, V. S.; Bashir, A. K. H.; Maaza, M.; Kaviyarasu, K.; Arasu, M. V.; Al-Dhabi, N. A.; Ignacimuthu, S. Biopolymeric Nanocomposite Scaffolds for Bone Tissue Engineering Applications − A Review. *J. Drug Delivery Sci. Technol.* **2020**, *55*, 101452.

(5) Rezwan, K.; Chen, Q. Z.; Blaker, J. J.; Boccaccini, A. R. Biodegradable and Bioactive Porous Polymer/Inorganic Composite Scaffolds for Bone Tissue Engineering. *Biomaterials* **2006**, *27* (18), 3413−3431.

(6) Kim, S. S.; Park, M. S.; Jeon, O.; Choi, C. Y.; Kim, B. S. Poly(Lactide-Co-Glycolide)/Hydroxyapatite Composite Scaffolds for Bone Tissue Engineering. *Biomaterials* **2006**, *27* (8), 1399−1409.

(7) Bohner, M.; Galea, L.; Doebelin, N. Calcium Phosphate Bone Graft Substitutes: Failures and Hopes. *J. Eur. Ceram. Soc.* **2012**, *32* (11), 2663−2671.

(8) Inzana, J. A.; Olvera, D.; Fuller, S. M.; Kelly, J. P.; Graeve, O. A.; Schwarz, E. M.; Kates, S. L.; Awad, H. A. 3D Printing of Composite Calcium Phosphate and Collagen Scaffolds for Bone Regeneration. *Biomaterials* **2014**, *35* (13), 4026−4034.

(9) Wahl, D. A.; Czernuszka, J. T. Collagen-Hydroxyapatite Composites for Hard Tissue Repair. *Eur. Cells Mater.* **2006**, *11*, 43−56.

(10) Thein-Han, W. W.; Misra, R. D. K. Biomimetic Chitosan-Nanohydroxyapatite Composite Scaffolds for Bone Tissue Engineering. *Acta Biomater.* **2009**, *5* (4), 1182−1197.

(11) Venkatesan, J.; Kim, S. K. Chitosan Composites for Bone Tissue Engineering-An Overview. *Mar. Drugs* **2010**, *8* (8), 2252−2266.

(12) Luo, Y. X.; Lode, A.; Sonntag, F.; Nies, B.; Gelinsky, M. Well-Ordered Biphasic Calcium Phosphate-Alginate Scaffolds Fabricated by Multi-Channel 3D Plotting under Mild Conditions. *J. Mater. Chem. B* **2013**, *1* (33), 4088−4098.

(13) Venkatesan, J.; Bhatnagar, I.; Manivasagan, P.; Kang, K. H.; Kim, S. K. Alginate Composites for Bone Tissue Engineering: A Review. *Int. J. Biol. Macromol.* **2015**, *72*, 269−281.

(14) Azevedo, M. C.; Reis, R. L.; Claase, B. M.; Grijpma, D. W.; Feijen, J. Development and Properties of Polycaprolactone/Hydroxyapatite Composite Biomaterials. *J. Mater. Sci.: Mater. Med.* **2003**, *14* (2), 103−107.

(15) De Santis, R.; Gloria, A.; Russo, T.; D'Amora, U.; D'Anto, V.; Bollino, F.; Catauro, M.; Mollica, F.; Rengo, S.; Ambrosio, L. Advanced Composites for Hard-Tissue Engineering Based on PCL/Organic-Inorganic Hybrid Fillers: From the Design of 2D Substrates to 3D Rapid Prototyped Scaffolds. *Polym. Compos.* **2013**, *34* (9), 1413−1417.

(16) Cui, Y.; Liu, Y.; Cui, Y.; Jing, X. B.; Zhang, P. B. A.; Chen, X. S. The Nanocomposite Scaffold of Poly(Lactide-Co-Glycolide) and Hydroxyapatite Surface-Grafted with L-Lactic Acid Oligomer for Bone Repair. *Acta Biomater.* **2009**, *5* (7), 2680−2692.

(17) Takayama, T.; Todo, M. Improvement of Mechanical Properties of Hydroxyapatite Particle-Filled Poly(L-Lactide) Biocomposites Using Lysine Tri-Isocyanate. *J. Mater. Sci.* **2009**, *44* (18), 5017−5020.

(18) Aydin, E.; Planell, J. A.; Hasirci, V. Hydroxyapatite Nanorod-Reinforced Biodegradable Poly(L-Lactic Acid) Composites for Bone Plate Applications. *J. Mater. Sci.: Mater. Med.* **2011**, *22* (11), 2413−2427.

(19) Venkatesan, J.; Kim, S.-K. Nano-Hydroxyapatite Composite Biomaterials for Bone Tissue Engineering-A Review. *J. Biomed. Nanotechnol.* **2014**, *10* (10), 3124−3140.

(20) Boissard, C. I. R.; Bourban, P. E.; Tami, A. E.; Alini, M.; Eglin, D. Nanohydroxyapatite/Poly(Ester Urethane) Scaffold for Bone Tissue Engineering. *Acta Biomater.* **2009**, *5* (9), 3316−3327.

(21) Yoshii, T.; Dumas, J. E.; Okawa, A.; Spengler, D. M.; Guelcher, S. A. Synthesis, Characterization of Calcium Phosphates/Polyurethane Composites for Weight-Bearing Implants. *J. Biomed. Mater. Res., Part B* **2012**, *100B* (1), 32−40.

(22) Li, K.; Yeung, C. Y.; Yeung, K. W. K.; Tjong, S. C. Sintered Hydroxyapatite/Polyetheretherketone Nanocomposites: Mechanical Behavior and Biocompatibility. *Adv. Eng. Mater.* **2012**, *14* (4), B155−B165.

(23) Shen, Q. Q.; Pan, Y. S. Tensile Mechanical Properties of Functional Gradient Hydroxyapatite/Polyether-Ether-Ketone Biocomposites. *Asian J. Chem.* **2014**, *26* (6), 1714−1716.
(24) Wong, K. L.; Wong, C. T.; Liu, W. C.; Pan, H. B.; Fong, M. K.; Lam, W. M.; Cheung, W. L.; Tang, W. M.; Chiu, K. Y.; Luk, K. D. K.; Lu, W. W. Mechanical Properties and *in Vitro* Response of Strontium-Containing Hydroxyapatite/Polyetheretherketone Composites. *Biomaterials* **2009**, *30* (23−24), 3810−3817.
(25) Lei, L. J.; Li, L.; Zhang, L. Q.; Chen, D. F.; Tian, W. Structure and Performance of Nano-Hydroxyapatite Filled Biodegradable Poly((1,2-Propanediol-Sebacate)-Citrate) Elastomers. *Polym. Degrad. Stab.* **2009**, *94* (9), 1494−1502.
(26) Jiang, L.; Li, Y.; Wang, X.; Zhang, L.; Wen, J.; Gong, M. Preparation and Properties of Nano-Hydroxyapatite/Chitosan/Carboxymethyl Cellulose Composite Scaffold. *Carbohydr. Polym.* **2008**, *74* (3), 680−684.
(27) Sadat-Shojai, M.; Khorasani, M.-T.; Dinpanah-Khoshdargi, E.; Jamshidi, A. Synthesis Methods for Nanosized Hydroxyapatite with Diverse Structures. *Acta Biomater.* **2013**, *9* (8), 7591−7621.
(28) Wegst, U. G. K.; Bai, H.; Saiz, E.; Tomsia, A. P.; Ritchie, R. O. Bioinspired Structural Materials. *Nat. Mater.* **2015**, *14* (1), 23−36.
(29) Landis, W. J.; Song, M. J.; Leith, A.; McEwen, L.; McEwen, B. F. Mineral and Organic Matrix Interaction in Normally Calcifying Tendon Visualized in Three Dimensions by High-Voltage Electron Microscopic Tomography and Graphic Image Reconstruction. *J. Struct. Biol.* **1993**, *110* (1), 39−54.
(30) Fratzl, P.; Weinkamer, R. Nature's Hierarchical Materials. *Prog. Mater. Sci.* **2007**, *52* (8), 1263−1334.
(31) Castro, A. G. B.; Polini, A.; Azami, Z.; Leeuwenburgh, S. C. G.; Jansen, J. A.; Yang, F.; van den Beucken, J. Incorporation of PLLA Micro-Fillers for Mechanical Reinforcement of Calcium-Phosphate Cement. *J. Mech. Behav. Biomed.* **2017**, *71*, 286−294.
(32) Kucko, N. W.; Schickert, S. D.; Marques, T. S.; Herber, R. P.; Van den Beuken, J.; Yi, Z.; Leeuwenburgh, S. C. G. Tough and Osteocompatible Calcium Phosphate Cements Reinforced with Poly(Vinyl Alcohol) Fibers. *ACS Biomater. Sci. Eng.* **2019**, *5* (5), 2491−2505.
(33) Paknahad, A.; Petre, D. G.; Leeuwenburgh, S. C. G.; Sluys, L. J. Interfacial Characterization of Poly (Vinyl Alcohol) Fibers Embedded in a Calcium Phosphate Cement Matrix: An Experimental and Numerical Investigation. *Acta Biomater.* **2019**, *96*, 582−593.
(34) Lausch, A. J.; Chong, L. C.; Uludag, H.; Sone, E. D. Multiphasic Collagen Scaffolds for Engineered Tissue Interfaces. *Adv. Funct. Mater.* **2018**, *28* (48), 1804730.
(35) Thrivikraman, G.; Athirasala, A.; Gordon, R.; Zhang, L. M.; Bergan, R.; Keene, D. R.; Jones, J. M.; Xie, H.; Chen, Z. Q.; Tao, J. H.; Wingender, B.; Gower, L.; Ferracane, J. L.; Bertassoni, L. E. Rapid Fabrication of Vascularized and Innervated Cell-Laden Bone Models with Biomimetic Intrafibrillar Collagen Mineralization. *Nat. Commun.* **2019**, *10*, DOI: 10.1038/s41467-019-11455-8.
(36) Cai, X.; Tong, H.; Shen, X. Y.; Chen, W. X.; Yan, J.; Hu, J. M. Preparation and Characterization of Homogeneous Chitosan-Polylactic Acid/Hydroxyapatite Nanocomposite for Bone Tissue Engineering and Evaluation of Its Mechanical Properties. *Acta Biomater.* **2009**, *5* (7), 2693−2703.
(37) Kaczmarek, B.; Sionkowska, A.; Osyczka, A. M. The Application of Chitosan/Collagen/Hyaluronic Acid Sponge Cross-Linked by Dialdehyde Starch Addition As a Matrix for Calcium Phosphate *via* Precipitation. *Int. J. Biol. Macromol.* **2018**, *107*, 470−477.
(38) Habibovic, P.; Barralet, J. E. Bioinorganics and Biomaterials: Bone Repair. *Acta Biomater.* **2011**, *7* (8), 3013−3026.
(39) Tite, T.; Popa, A. C.; Balescu, L. M.; Bogdan, I. M.; Pasuk, I.; Ferreira, J. M. F.; Stan, G. E. Cationic Substitutions in Hydroxyapatite: Current Status of the Derived Biofunctional Effects and Their *in Vitro* Interrogation Methods. *Materials* **2018**, *11* (11), 62.
(40) Yang, F.; Yang, D.; Tu, J.; Zheng, Q.; Cai, L.; Wang, L. Strontium Enhances Osteogenic Differentiation of Mesenchymal Stem Cells and *in Vivo* Bone Formation by Activating Wnt/Catenin Signaling. *Stem Cells* **2011**, *29* (6), 981−991.
(41) Capuccini, C.; Torricelli, P.; Sima, F.; Boanini, E.; Ristoscu, C.; Bracci, B.; Socol, G.; Fini, M.; Mihailescu, I. N.; Bigi, A. Strontium-Substituted Hydroxyapatite Coatings Synthesized by Pulsed-Laser Deposition: *In Vitro* Osteoblast and Osteoclast Response. *Acta Biomater.* **2008**, *4* (6), 1885−1893.
(42) Wu, C. T.; Zhou, Y. H.; Xu, M. C.; Han, P. P.; Chen, L.; Chang, J.; Xiao, Y. Copper-Containing Mesoporous Bioactive Glass Scaffolds with Multifunctional Properties of Angiogenesis Capacity, Osteostimulation and Antibacterial Activity. *Biomaterials* **2013**, *34* (2), 422−433.
(43) Bari, A.; Bloise, N.; Fiorilli, S.; Novajra, G.; Vallet-Regi, M.; Bruni, G.; Torres-Pardo, A.; Gonzalez-Calbet, J. M.; Visai, L.; Vitale-Brovarone, C. Copper-Containing Mesoporous Bioactive Glass Nanoparticles As Multifunctional Agent for Bone Regeneration. *Acta Biomater.* **2017**, *55*, 493−504.
(44) Hausmann, M. K.; Rühs, P. A.; Siqueira, G.; Läuger, J.; Libanori, R.; Zimmermann, T.; Studart, A. R. Dynamics of Cellulose Nanocrystal Alignment During 3D Printing. *ACS Nano* **2018**, *12* (7), 6926−6937.
(45) Lewicki, J. P.; Rodriguez, J. N.; Zhu, C.; Worsley, M. A.; Wu, A. S.; Kanarska, Y.; Horn, J. D.; Duoss, E. B.; Ortega, J. M.; Elmer, W.; Hensleigh, R.; Fellini, R. A.; King, M. J. 3D-Printing of Meso-Structurally Ordered Carbon Fiber/Polymer Composites with Unprecedented Orthotropic Physical Properties. *Sci. Rep.* **2017**, *7*, srep43401.
(46) Farah, S.; Anderson, D. G.; Langer, R. Physical and Mechanical Properties of PLA, and Their Functions in Widespread Applications — A Comprehensive Review. *Adv. Drug Delivery Rev.* **2016**, *107*, 367−392.
(47) Hench, L. L. Bioceramics. *J. Am. Ceram. Soc.* **1998**, *81* (7), 1705−1728.
(48) Fu, Q.; Saiz, E.; Rahaman, M. N.; Tomsia, A. P. Bioactive Glass Scaffolds for Bone Tissue Engineering: State of the Art and Future Perspectives. *Mater. Sci. Eng., C* **2011**, *31* (7), 1245−1256.
(49) Pietrzak, W. S.; Sarver, D. R.; Verstynen, M. L. Bioabsorbable Polymer Science for the Practicing Surgeon. *J. Craniofac. Surg.* **1997**, *8* (2), 87−91.
(50) Salgado, A. J.; Coutinho, O. P.; Reis, R. L. Bone Tissue Engineering: State of the Art and Future Trends. *Macromol. Biosci.* **2004**, *4* (8), 743−765.
(51) Sarker, M.; Izadifar, M.; Schreyer, D.; Chen, X. Influence of Ionic Crosslinkers (Ca^{2+}/Ba^{2+}/Zn^{2+}) on the Mechanical and Biological Properties of 3D Bioplotted Hydrogel Scaffolds. *J. Biomater. Sci., Polym. Ed.* **2018**, *29* (10), 1126−1154.
(52) Zhang, B.; Wang, L.; Song, P.; Pei, X.; Sun, H.; Wu, L.; Zhou, C.; Wang, K.; Fan, Y.; Zhang, X. 3D Printed Bone Tissue Regenerative PLA/HA Scaffolds with Comprehensive Performance Optimizations. *Mater. Des.* **2021**, *201*, 109490.
(53) Kareem, M. M.; Tanner, K. E. Optimising Micro-Hydroxyapatite Reinforced Poly(Lactide Acid) Electrospun Scaffolds for Bone Tissue Engineering. *J. Mater. Sci.: Mater. Med.* **2020**, *31* (4), 38.
(54) Kutikov, A. B.; Gurijala, A.; Song, J. Rapid Prototyping Amphiphilic Polymer/Hydroxyapatite Composite Scaffolds with Hydration-Induced Self-Fixation Behavior. *Tissue Eng., Part C* **2015**, *21* (3), 229−241.
(55) Rong, Z.; Zeng, W.; Kuang, Y.; Zhang, J.; Liu, X.; Lu, Y.; Cheng, X. Enhanced Bioactivity of Osteoblast-Like Cells on Poly(Lactic Acid)/Poly(Methyl Methacrylate)/Nano-Hydroxyapatite Scaffolds for Bone Tissue Engineering. *Fibers Polym.* **2015**, *16* (2), 245−253.
(56) Wang, R. Z.; Gupta, H. S. Deformation and Fracture Mechanisms of Bone and Nacre. *Annu. Rev. Mater. Res.* **2011**, *41*, 41−73.
(57) Zhou, S.; Zheng, X.; Yu, X.; Wang, J.; Weng, J.; Li, X.; Feng, B.; Yin, M. Hydrogen Bonding Interaction of Poly(D,L-Lactide)/Hydroxyapatite Nanocomposites. *Chem. Mater.* **2007**, *19* (2), 247−253.

(58) Kepa, K.; Coleman, R.; Grøndahl, L. *In Vitro* Mineralization of Functional Polymers. *Biosurface Biotribology* **2015**, *1* (3), 214−227.
(59) Yang, K.; Wei, J.; Wang, C.; Li, Y. A Study on *in Vitro* and *in Vivo* Bioactivity of Nano Hydroxyapatite/Polymer Biocomposite. *Chin. Sci. Bull.* **2007**, *52* (2), 267−271.
(60) Lao, L.; Wang, Y.; Zhu, Y.; Zhang, Y.; Gao, C. Poly(Lactide-Co-Glycolide)/Hydroxyapatite Nanofibrous Scaffolds Fabricated by Electrospinning for Bone Tissue Engineering. *J. Mater. Sci.: Mater. Med.* **2011**, *22* (8), 1873−1884.
(61) Zhang, H.; Fu, Q.-W.; Sun, T.-W.; Chen, F.; Qi, C.; Wu, J.; Cai, Z.-Y.; Qian, Q.-R.; Zhu, Y.-J. Amorphous Calcium Phosphate, Hydroxyapatite and Poly(D,L-Lactic Acid) Composite Nanofibers: Electrospinning Preparation, Mineralization and *in Vivo* Bone Defect Repair. *Colloids Surf., B* **2015**, *136*, 27−36.
(62) Barralet, J.; Gbureck, U.; Habibovic, P.; Vorndran, E.; Gerard, C.; Doillon, C. J. Angiogenesis in Calcium Phosphate Scaffolds by Inorganic Copper Ion Release. *Tissue Eng., Part A* **2009**, *15* (7), 1601−1609.
(63) Erol, M. M.; Mouriño, V.; Newby, P.; Chatzistavrou, X.; Roether, J. A.; Hupa, L.; Boccaccini, A. R. Copper-Releasing, Boron-Containing Bioactive Glass-Based Scaffolds Coated with Alginate for Bone Tissue Engineering. *Acta Biomater.* **2012**, *8* (2), 792−801.
(64) Yang, Y.; Zheng, K.; Liang, R.; Mainka, A.; Taccardi, N.; Roether, J. A.; Detsch, R.; Goldmann, W. H.; Virtanen, S.; Boccaccini, A. R. Cu-Releasing Bioactive Glass/Polycaprolactone Coating on Mg with Antibacterial and Anticorrosive Properties for Bone Tissue Engineering. *Biomed. Mater.* **2018**, *13* (1), 015001.
(65) Cao, B.; Zheng, Y.; Xi, T.; Zhang, C.; Song, W.; Burugapalli, K.; Yang, H.; Ma, Y. Concentration-Dependent Cytotoxicity of Copper Ions on Mouse Fibroblasts *in Vitro*: Effects of Copper Ion Release from Tcu380a Vs Tcu220c Intra-Uterine Devices. *Biomed. Microdevices* **2012**, *14* (4), 709−720.
(66) Huang, Y.; Hao, M.; Nian, X.; Qiao, H.; Zhang, X.; Zhang, X.; Song, G.; Guo, J.; Pang, X.; Zhang, H. Strontium and Copper Co-Substituted Hydroxyapatite-Based Coatings with Improved Antibacterial Activity and Cytocompatibility Fabricated by Electrodeposition. *Ceram. Int.* **2016**, *42* (10), 11876−11888.
(67) Weng, L.; Boda, S. K.; Teusink, M. J.; Shuler, F. D.; Li, X. R.; Xie, J. W. Binary Doping of Strontium and Copper Enhancing Osteogenesis and Angiogenesis of Bioactive Glass Nanofibers While Suppressing Osteoclast Activity. *ACS Appl. Mater. Interfaces* **2017**, *9* (29), 24484−24496.
(68) Huang, Y.; Zhou, G.; Zheng, L.; Liu, H.; Niu, X.; Fan, Y. Micro-/Nano- Sized Hydroxyapatite Directs Differentiation of Rat Bone Marrow Derived Mesenchymal Stem Cells towards an Osteoblast Lineage. *Nanoscale* **2012**, *4* (7), 2484−2490.
(69) Yang, X.; Li, Y.; Liu, X.; Zhang, R.; Feng, Q. *In Vitro* Uptake of Hydroxyapatite Nanoparticles and Their Effect on Osteogenic Differentiation of Human Mesenchymal Stem Cells. *Stem Cells Int.* **2018**, *2018*, 2036176.
(70) Matsugaki, A.; Isobe, Y.; Saku, T.; Nakano, T. Quantitative Regulation of Bone-Mimetic, Oriented Collagen/Apatite Matrix Structure Depends on the Degree of Osteoblast Alignment on Oriented Collagen Substrates. *J. Biomed. Mater. Res., Part A* **2015**, *103* (2), 489−499.
(71) Wu, V.; van Oers, R. F. M.; Schulten, E. A. J. M.; Helder, M. N.; Bacabac, R. G.; Klein-Nulend, J. Osteocyte Morphology and Orientation in Relation to Strain in the Jaw Bone. *Int. J. Oral Sci.* **2018**, *10* (1), 2.
(72) Kerschnitzki, M.; Wagermaier, W.; Roschger, P.; Seto, J.; Shahar, R.; Duda, G. N.; Mundlos, S.; Fratzl, P. The Organization of the Osteocyte Network Mirrors the Extracellular Matrix Orientation in Bone. *J. Struct. Biol.* **2011**, *173* (2), 303−311.
(73) Zhu, B. S.; Lu, Q. H.; Yin, J.; Hu, J.; Wang, Z. G. Alignment of Osteoblast-Like Cells and Cell-Produced Collagen Matrix Induced by Nanogrooves. *Tissue Eng.* **2005**, *11* (5−6), 825−834.
(74) Kulangara, K.; Yang, Y.; Yang, J.; Leong, K. W. Nanotopography as Modulator of Human Mesenchymal Stem Cell Function. *Biomaterials* **2012**, *33* (20), 4998−5003.
(75) Lee, K.; Kim, E. H.; Oh, N.; Tuan, N. A.; Bae, N. H.; Lee, S. J.; Lee, K. G.; Eom, C.-Y.; Yim, E. K.; Park, S. Contribution of Actin Filaments and Microtubules to Cell Elongation and Alignment Depends on the Grating Depth of Micrograting. *J. Nanobiotechnol.* **2016**, *14* (1), 35.
(76) Mathieu, P. S.; Loboa, E. G. Cytoskeletal and Focal Adhesion Influences on Mesenchymal Stem Cell Shape, Mechanical Properties, and Differentiation Down Osteogenic, Adipogenic, and Chondrogenic Pathways. *Tissue Eng., Part B* **2012**, *18* (6), 436−444.
(77) Teo, B. K. K.; Wong, S. T.; Lim, C. K.; Kung, T. Y. S.; Yap, C. H.; Ramagopal, Y.; Romer, L. H.; Yim, E. K. F. Nanotopography Modulates Mechanotransduction of Stem Cells and Induces Differentiation through Focal Adhesion Kinase. *ACS Nano* **2013**, *7* (6), 4785−4798.
(78) Yim, E. K. F.; Pang, S. W.; Leong, K. W. Synthetic Nanostructures Inducing Differentiation of Human Mesenchymal Stem Cells into Neuronal Lineage. *Exp. Cell Res.* **2007**, *313* (9), 1820−1829.
(79) Namgung, S.; Baik, K. Y.; Park, J.; Hong, S. Controlling the Growth and Differentiation of Human Mesenchymal Stem Cells by the Arrangement of Individual Carbon Nanotubes. *ACS Nano* **2011**, *5* (9), 7383−7390.
(80) Ozguldez, H. O.; Cha, J.; Hong, Y.; Koh, I.; Kim, P. Nanoengineered, Cell-Derived Extracellular Matrix Influences ECM-Related Gene Expression of Mesenchymal Stem Cells. *Biomater. Res.* **2018**, *22* (1), 32.
(81) Shin, Y. M.; Shin, H. J.; Yang, D.-H.; Koh, Y.-J.; Shin, H.; Chun, H. J. Advanced Capability of Radially Aligned Fibrous Scaffolds Coated with Polydopamine for Guiding Directional Migration of Human Mesenchymal Stem Cells. *J. Mater. Chem. B* **2017**, *5* (44), 8725−8737.
(82) Tijore, A.; Irvine, S. A.; Sarig, U.; Mhaisalkar, P.; Baisane, V.; Venkatraman, S. Contact Guidance for Cardiac Tissue Engineering Using 3D Bioprinted Gelatin Patterned Hydrogel. *Biofabrication* **2018**, *10* (2), 025003.
(83) Delon, I.; Brown, N. H. Integrins and the Actin Cytoskeleton. *Curr. Opin. Cell Biol.* **2007**, *19* (1), 43−50.
(84) Wiesner, S.; Legate, K. R.; Fässler, R. Integrin-Actin Interactions. *Cell. Mol. Life Sci.* **2005**, *62* (10), 1081−1099.

https://doi.org/10.1021/acsnano.1c03905
ACS Nano 2021, 15, 17480−17498